

---

# Analysis of Geodetic Time Series Using Allan Variances



Studienarbeit im Studiengang  
**Geodäsie und Geoinformatik**  
an der Universität Stuttgart

Thomas Friederichs

Stuttgart, November 2010

---

**Betreuer:** Prof. Dr.-Ing. Nico Sneeuw  
Universität Stuttgart



# Erklärung der Urheberschaft

Ich erkläre hiermit an Eides statt, dass ich die vorliegende Arbeit ohne Hilfe Dritter und ohne Benutzung anderer als der angegebenen Hilfsmittel angefertigt habe; die aus fremden Quellen direkt oder indirekt übernommenen Gedanken sind als solche kenntlich gemacht. Die Arbeit wurde bisher in gleicher oder ähnlicher Form in keiner anderen Prüfungsbehörde vorgelegt und auch noch nicht veröffentlicht.

Ort, Datum

Unterschrift



# Summary

The Allan variance is a statistical measure, developed in the 1960's by the American physicist David W. Allan. With its aid, data series measured by devices like oscillators or gyroscopes can be analyzed with regard to their stability. In contrast to the Allan variance, the standard variance as a measure of total signal power, is not able to characterize signal stability.

There exist further developments of the Allan variance. This student research project considers mainly non-overlapping, overlapping and modified Allan variances.

The result of an Allan variance computation is the so-called  $\sigma$ - $\tau$ -diagram. This diagram provides information about the stability and beyond, it allows identification of various random processes that exist in the series of measurement.

The Allan variance may be computed directly in the time domain as well as via the frequency domain using the power spectral density of the time series and a transfer function.

A domain conversion between the Allan variance and the power spectral density is only unidirectional. More precisely, one can compute the Allan variance by means of the power spectral density, but not vice versa.

This student research project takes up the challenge of applying the concept of the Allan variance to geodetic time series (pole coordinates as part of the Earth orientation parameters, GPS measured coordinates of one position, Scintrex CG-5 gravimeter data and GOCE gravity gradients, in addition to oscillator frequencies).

The Allan variance turns out to be a reasonable statistical measure for analysis of geodetic time series. The Allan variance, or better the Allan deviation, especially in an entire diagram, can be considered as a form of spectral analysis. Having said this, it is possible to consider the averaging interval  $\tau$  as the inverted frequency.



# Contents

<b>1</b>	<b>Introduction</b>	<b>1</b>
<b>2</b>	<b>Time Domain Stability Analysis</b>	<b>3</b>
2.1	Timing Signal Model . . . . .	3
2.2	Variances . . . . .	5
2.2.1	Standard Variance . . . . .	5
2.2.2	Allan Variance . . . . .	6
2.2.3	Overlapping Allan Variance . . . . .	8
2.2.4	Modified Allan Variance . . . . .	10
2.2.5	Overview of developed variances . . . . .	10
2.3	The result of an Allan variance computation . . . . .	11
2.3.1	The Sigma-Tau-Diagram . . . . .	14
2.3.2	Comparison of three different Allan variance plots on the basis of a show- case data set . . . . .	14
2.3.3	Computation times . . . . .	17
2.3.4	Accuracy versus Stability . . . . .	18
<b>3</b>	<b>Frequency Domain Stability Analysis</b>	<b>19</b>
3.1	Noise Spectra . . . . .	19
3.2	Spectral Analysis . . . . .	22
3.3	Domain Conversions . . . . .	22
<b>4</b>	<b>Application to geodetic time series</b>	<b>25</b>
4.1	Oscillator frequencies . . . . .	26
4.2	Earth Orientation Parameters: Pole coordinates . . . . .	29
4.2.1	$x$ -component of pole coordinates . . . . .	30
4.2.2	$y$ -component of pole coordinates . . . . .	32
4.3	GPS measured coordinates . . . . .	33
4.3.1	Absolute values of complex GPS position data . . . . .	35
4.3.2	Arguments of complex GPS position data . . . . .	36
4.4	Scintrex CG-5 Gravimeter data . . . . .	37
4.5	GOCE gravity gradients . . . . .	40
4.5.1	GOCE gravity gradients $T_{xx}$ , $T_{yy}$ and $T_{zz}$ . . . . .	40
4.5.2	GOCE gravity gradients $T_{xy}$ . . . . .	47
<b>5</b>	<b>Discussion</b>	<b>49</b>
<b>A</b>	<b>Appendix</b>	<b>XV</b>
<b>B</b>	<b>Appendix</b>	<b>XVII</b>

<b>C</b>	<b>Appendix</b>	<b>XXI</b>
C.1	Calculation of the sigma-tau diagrams for non-overlapping, overlapping and modified Allan deviation (Time-Domain-Based) . . . . .	XXI
C.2	Calculation of the sigma-tau diagrams for overlapping and modified Allan deviation (Frequency-Domain-Based) . . . . .	XXI
C.3	Main programs for the analysis of geodetic time series . . . . .	XXI
C.4	Additional helper functions . . . . .	XXII

## List of Figures

1.1	Example for random processes, for which the standard deviation does not converge . . . . .	2
2.1	Sampling time, observation time and dead time. . . . .	4
2.2	Simulated time deviation $x(t)$ and fractional frequency plot $y(t)$ . . . . .	7
2.3	Comparison of non-overlapping and overlapping sampling . . . . .	8
2.4	Derivation model for the overlapping Allan variance . . . . .	9
2.5	Frequency values of an oscillator in one-second cycles . . . . .	12
2.6	Frequency values of an oscillator in two-second cycles . . . . .	12
2.7	Frequency data of an oscillator . . . . .	14
2.8	$\sigma$ - $\tau$ diagram with non-overlapping Allan deviation on the basis of oscillator data	15
2.9	$\sigma$ - $\tau$ diagram with overlapping Allan deviation on the basis of oscillator data . . .	15
2.10	$\sigma$ - $\tau$ diagram with modified Allan deviation on the basis of oscillator data . . . .	16
2.11	Accuracy and stability are not the same! . . . . .	18
3.1	Noise type and time series for a set of simulated phase data. . . . .	20
3.2	Slopes of common power law noise processes . . . . .	21
3.3	Transfer function of the Allan (two-sample) time domain stability . . . . .	23
3.4	Overview of domain conversions . . . . .	24
4.1	Frequency data of a 10 MHz reference of an Agilent N9020A spectrum analyzer .	26
4.2	$\sigma$ - $\tau$ -diagram with Allan deviations for analyzed oscillator . . . . .	27
4.3	$\sigma$ - $\tau$ -diagram with modified Allan deviations for analyzed oscillator . . . . .	28
4.4	Polar motion from 1990 up to 2007 . . . . .	29
4.5	x-coordinate of pole from 1990 up to 2007 . . . . .	30
4.6	$\sigma$ - $\tau$ -diagram with Allan deviations for x-coordinates of pole . . . . .	30
4.7	$\sigma$ - $\tau$ -diagram with modified Allan deviations for x-coordinates of pole . . . . .	31
4.8	y-coordinate of pole from 1990 up to 2007 . . . . .	32
4.9	$\sigma$ - $\tau$ -diagram with Allan deviations for y-coordinates of pole . . . . .	32
4.10	$\sigma$ - $\tau$ -diagram with modified Allan deviations for y-coordinates of pole . . . . .	33
4.11	Scatter plot of GPS measured position data . . . . .	34
4.12	A complex number in the complex plane . . . . .	34
4.13	Time series with absolute values of complex GPS position data . . . . .	35
4.14	$\sigma$ - $\tau$ -diagrams for absolute values . . . . .	35
4.15	Time series with arguments of complex GPS position data . . . . .	36
4.16	$\sigma$ - $\tau$ -diagrams for arguments . . . . .	36
4.17	Preprocessed gravimeter data . . . . .	37
4.18	$\sigma$ - $\tau$ -diagram with Allan deviations for gravimeter data . . . . .	38
4.19	$\sigma$ - $\tau$ -diagram with modified Allan deviations for gravimeter data . . . . .	38
4.20	Difference in ADEV computation between trend reduced and trend affected data	39

4.21	Gravity gradients in along track direction and an appropriate Fourier series . . .	41
4.22	Reduced gravity gradients in along track direction . . . . .	41
4.23	Original and reduced gravity gradients of the three main diagonal terms $T_{xx}$ , $T_{yy}$ and $T_{zz}$ . . . . .	43
4.24	$\sigma$ - $\tau$ -diagrams of the three main diagonal terms $T_{xx}$ , $T_{yy}$ and $T_{zz}$ . . . . .	44
4.25	Original gravity gradients of the three main diagonal terms $T_{xx}$ , $T_{yy}$ , $T_{zz}$ and their corresponding time-domain based sigma-tau plots . . . . .	45
4.26	Original gravity gradients of the three main diagonal terms $T_{xx}$ , $T_{yy}$ , $T_{zz}$ and their corresponding sigma-tau plots via PSD and transfer function . . . . .	46
4.27	Original and reduced gravity gradients of the off-diagonal term $T_{xy}$ . . . . .	47
4.28	$\sigma$ - $\tau$ -diagrams of the off-diagonal term $T_{xy}$ . . . . .	48
4.29	$\sigma$ - $\tau$ -diagrams of the off-diagonal term $T_{xy}$ . . . . .	48
B.1	Sinus signal . . . . .	XVII
B.2	sigma-tau plot for the sinus signal . . . . .	XVIII
B.3	Graphical solution of the determination of the maximum . . . . .	XIX

## List of Tables

2.1	Overview of developed variances . . . . .	11
2.2	Results of Allan deviation computation using oscillator frequency data . . . . .	17
2.3	CPU times . . . . .	17
3.1	Noise types with corresponding exponent . . . . .	19
3.2	Spectral characteristics of power law noise processes . . . . .	21



# Chapter 1

## Introduction

Prior to mathematically deriving, describing and applying of the Allan variance on geodetic time series, it is reasonable to mention the original field of application of the Allan variance and to put it in historical context.

In horology it is coercively necessary to carry out stability analysis. Using clocks, i.e. frequency normals, one has to act on the assumption that their nominal frequency remains stable over long time periods.

The field of modern frequency stability analysis began in the mid 1960's with the emergence of improved analytical and measurement techniques. In particular, new statistics became available that were better suited for common clock noises than the classic N-sample variance, and better methods were developed for high resolution measurements. A seminal conference on short-term stability in 1964, and the introduction of the two-sample (Allan<sup>1</sup>) variance in 1966 marked the beginning of this new era, which was summarized in a special issue of the Proceedings of the IEEE in 1966 [1]. This period also marked the introduction of commercial atomic frequency standards. The subsequent advances in the performance of frequency sources depended largely on the improved ability to measure and analyze their stability [2].

It is worth mentioning that the progress in frequency stability analysis is still going on. From 1966 (two-sample Allan variance) up to now (ThêoH), a lot of variances and therefore new statistical measures have been developed. During this progress the original Allan variance has been improved and in this context also the statistical confidence for one and the same data set. With regard to horology these improvements are due to the extension to longer averaging time, which provides better long-term clock characterization. The goal is to extract the maximum information content out of a data set without the time and expense of a longer data record [3]. This student research project focusses on non-overlapping, overlapping and modified Allan variance.

Before immediately plunging in medias res, some further introductory sentences should help understanding why there is a need for this statistical measure, named Allan variance.

For this purpose, one has to address the topic of frequency stability analysis. Suppose a flawless measuring device is available and measures the frequency of an oscillator within a measuring time of 1 s with arbitrary resolution. With this idealization, the measuring device would output measuring values of the frequency of that oscillator in cycles tuned to seconds. These values could be evaluated statistically. If one obtains always the same measuring value, then one has an ideal, infinite stable oscillator. But in reality, one does not always obtain the same frequency

---

<sup>1</sup>David W. Allan, physicist, born in Mapleton, Utah in 1936

value. The measuring values fluctuate around an average value with a certain width. Assuming the measuring device to be flawless, the fluctuations refer to the characteristics of the test item, and indicate that the stability of the oscillator is limited.

Now, calculating the mean of all frequency values would be the first idea of everybody who has ever dealt with statistics. It is self-evident to take the next step by calculating the variance and the standard deviation, too. These are statistical quantities that advise someone of the spread of the statistical distribution of the measuring values around the mean.

Indeed the standard deviation would seem to be an appropriate measure for stability. However, the American physicist David W. Allan found out the following: Among random processes being responsible for instabilities, there are some of them, for which the standard deviation does not converge anymore to a finite value, but become infinite, with increasing number of measuring values, if any of them is existent. The left part of Figure 1.1 shows an example for such random processes. Generally, any non-white FM noise process has convergence problems for the standard deviation. The right part of Figure 1.1 depicts the mentioned effect. The standard deviation (upper curve in blue) increases with the number of samples of flicker FM noise used to determine it, while the Allan deviation (lower curve in red) is essentially constant. The problem with the standard variance stems from its use of the deviations from the average, which is not stationary for the more divergence noise types.

Hence Allan realized that the standard deviation is not appropriate to describe correctly all types of random processes in a device like an oscillator. Consequently he developed the Allan variance named after him. This statistical measure shall be explained and applied to geodetic time series in the next chapters by means of MATLAB files that were developed in the course of this.

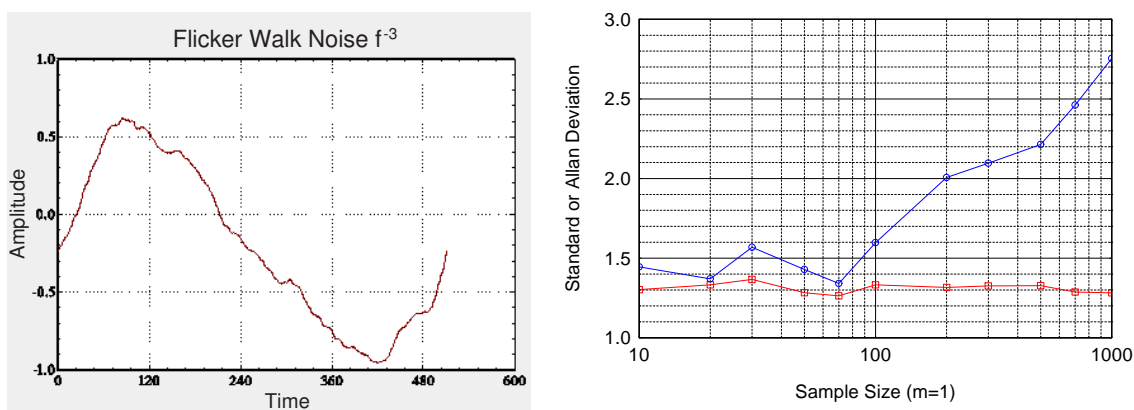


*Figure 1.1: Example for random processes, for which the standard deviation does not converge*

## Chapter 2

### Time Domain Stability Analysis

The stability of a frequency source in the time domain is based on the statistics of its phase or frequency fluctuations as a function of time, a form of time series analysis. This analysis generally uses some type of variance, a 2nd moment measure of the fluctuations. For many divergent noise types commonly associated with frequency sources, the standard variance, which is based on the variations around the average value, is not convergent, and thus, other variances have been developed as introduced in the following paragraphs [4, 5, 6, 7].

#### 2.1 Timing Signal Model

Before treating geodetic time series, we consider a frequency source like a clock i.e. an oscillator. We define the variables  $x(t)$  and  $y(t)$ , the phase and the fractional frequency, respectively. The fundamentals of frequency stability are derived from the clock model below.

$$V(t) = [V_0 + \epsilon(t)] \sin [2\pi\nu_0 t + \phi(t)], \quad (2.1)$$

with

- $V(t)$  : Actual clock output
- $V_0$  : Nominal peak output voltage
- $\epsilon(t)$  : Amplitude deviation
- $\nu_0$  : Nominal frequency in Hertz
- $\phi(t)$  : Phase deviation

The amplitude consisting of nominal peak voltage and amplitude deviation is not important in time-domain frequency analysis. We are concerned primarily with the  $\phi(t)$  term. The instantaneous frequency is the derivative of the total phase:

$$\nu(t) = \nu_0 + \frac{1}{2\pi} \frac{d\phi}{dt}. \quad (2.2)$$

For precision oscillators, we define the fractional frequency as

$$y(t) = \frac{\Delta f}{f} = \frac{\nu(t) - \nu_0}{\nu_0} = \frac{1}{2\pi\nu_0} \frac{d\phi}{dt} = \frac{dx}{dt}, \quad (2.3)$$

whereat

$$x(t) = \frac{\phi(t)}{2\pi\nu_0}. \quad (2.4)$$

Note that the fractional frequency  $y(t)$  is dimensionless because it is normalized to the nominal frequency  $\nu_0$ . Sometimes the term  $x(t)$  is also called random time deviation or time fluctuations.

The basis of a time domain stability analysis is an array of equally spaced phase or fractional frequency deviation data arrays,  $x_i$  and  $y_i$ , respectively, where the index  $i$  refers to data points in time. These data are equivalent, and conversions between them are possible. The  $x$  values have units of time in seconds, and the  $y$  values are (dimensionless) fractional frequency,  $\Delta f/f$ . The  $x(t)$  time fluctuations are related to the phase fluctuations by  $\phi(t) = x(t) \cdot 2\pi\nu_0$ . Both are commonly called "phase" to distinguish them from the independent time variable  $t$ . The data sampling or measurement interval  $\tau_0$  has units of seconds. The analysis or averaging time  $\tau$  – also called observation interval – may be a multiple of  $\tau_0$ :

$$\tau = m \cdot \tau_0, \text{ where } m \text{ is the averaging factor.} \quad (2.5)$$

Very widely used is the averaged sample of the normalized, fractional frequency  $y(t)$ . It is defined as

$$\bar{y}_i(\tau) = \frac{1}{\tau} \int_{t_i}^{t_i+\tau} y(t) dt \quad (2.6)$$

By considering a generic instant  $t_i$  we get from equation (2.3)

$$\bar{y}_i(\tau) = \frac{\phi(t_i + \tau) - \phi(t_i)}{2\pi\nu_0\tau} = \frac{x(t_i + \tau) - x(t_i)}{\tau}. \quad (2.7)$$

It is worthwhile remarking, that the operator in the discrete-time domain that corresponds to the derivative operator defined in the continuous-time domain is the *difference* operator. Taking the differences between adjacent data points plays an important role for performing phase to frequency data conversion, calculating Allan variances and later performing noise identification. The first difference  $y_i$  of a sequence of samples  $x_i$ , evenly spaced with sampling period  $T$  in the discrete-time domain is given by

$$\text{1st difference: } y_i = \frac{x_{i+1} - x_i}{T} \quad (2.8)$$

equivalent to the first derivative  $y(t) = x'(t)$  in the continuous-time domain. Analogously, the second difference  $z_i$  is given by

$$\text{2nd difference: } z_i = \frac{y_{i+1} - y_i}{T} = \frac{x_{i+2} - 2x_{i+1} + x_i}{T^2} \quad (2.9)$$

equivalent to the second derivative  $z(t) = y'(t) = x''(t)$ . The sampling period  $T$  means [8]:

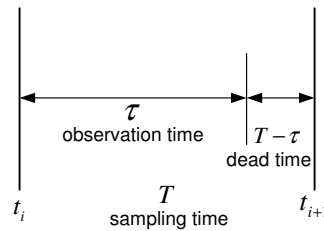


Figure 2.1: Sampling time, observation time and dead time.

In this paper the dead time between measurements is neglected, i.e.  $T - \tau = 0$ . Due to random fluctuations of  $y(t)$  in real oscillators or other time series, repeated measurements of  $\bar{y}_i$  yield random results (or better, different samples of a random variable). The fundamental issue of time and frequency characterization in the time domain is thus to identify suitable statistical measures of  $\bar{y}_i$ . In particular, a statistical measure of the dispersion of the  $y_i$  samples provides a time-domain measure of instability over  $\tau$ .

## 2.2 Variances

Variances are used to characterize the fluctuations of a frequency source. These are second-moment measures of scatter, much as the standard variance is used to quantify the variations around a nominal value. The variations from the mean are squared, summed, and divided by one less than the number of measurements. This number is called the *degrees of freedom*. Several statistical variances are available to the frequency stability analyst, and this section provides an overview of them. The attention is mainly on standard variance, Allan variance, overlapping Allan variance and modified Allan variance. The overview of all variance types at the end of this section is just for the sake of completeness.

### 2.2.1 Standard Variance

The classic N-sample or standard variance is defined [9] as

$$s^2 = \frac{1}{N-1} \sum_{i=1}^N (y_i - \bar{y})^2, \quad (2.10)$$

where the  $y_i$  are the  $N$  fractional frequency values, and  $\bar{y} = \frac{1}{N} \sum_{i=1}^N y_i$  is the average fractional frequency. The standard variance  $s^2$  and its square root  $s$  (standard deviation) are widely used statistical tools to measure the dispersion of samples of a random variable. In our case, under the assumption that  $y(t)$  is ergodic and has zero mean, the standard variance is simply equal to

$$s^2[y_i] = \langle \bar{y}_i^2 \rangle = I^2(\tau)^1 \quad (2.12)$$

This quantity is a theoretical measure and is based on averaging over all available samples. It is also denoted as  $I^2(\tau)$  because it indicates that it is a measure of *instability* over the time interval  $\tau$ . For stationary frequency fluctuations, the standard variance has the following limit values:

$$\lim_{\tau \rightarrow 0} I(\tau) = \sqrt{\langle y^2(t) \rangle} \quad (2.13)$$

$$\lim_{\tau \rightarrow \infty} I(\tau) = 0 \quad (2.14)$$

<sup>1</sup>The symbol  $\langle \cdot \rangle$  denotes the infinite time-average operator on the argument function. For example, in the case of continuous-time argument  $s(t)$ , it is defined as

$$\langle s(t) \rangle = \lim_{T \rightarrow \infty} \frac{1}{2T} \int_{-T}^T s(t) dt \quad (2.12)$$

In other words, for  $\tau \rightarrow 0$  we approach ideal instantaneous frequency measurement (yielding the root mean square value of  $y(t)$ ) and for  $\tau \rightarrow \infty$  stationary fluctuations tend to be completely averaged out. Despite its mathematical simplicity, the standard variance  $I^2(\tau)$  is really not a useful tool for stability characterization, because its time-averaging does not converge for some common kinds of phase noise, such as flicker and random-walk frequency noise (see 3.1 for common types of clock noise). In particular, the limit value for  $\tau \rightarrow \infty$  may approach infinity in such cases. Therefore, more suitable quantities for clock stability characterization were introduced beginning from 1966 by Allan and others to cope with such convergence issues in most cases of practical interest.

### 2.2.2 Allan Variance

The Allan variance is the most common time-domain measure of frequency stability. Similar to the standard variance it is a measure of the fractional frequency fluctuations, but has the advantage of being convergent for most types of clock noise. There are several versions for the Allan variance that provide better statistical confidence, can distinguish between white and flicker phase noise (see 3.1), and can describe time stability.

The original non-overlapping Allan, or two-sample variance, AVAR, is the standard time-domain measure of frequency stability. It is defined [4, 9] as

$$\sigma_y^2(\tau) = \frac{1}{2(M-1)} \sum_{i=1}^{M-1} [\bar{y}_{i+1} - \bar{y}_i]^2, \quad (2.15)$$

where  $\bar{y}_i$  is the  $i^{\text{th}}$  of  $M$  fractional frequency values averaged over the measurement (sampling) interval  $\tau$  according to equation (2.6). In terms of phase data, the Allan variance may be calculated as

$$\sigma_y^2(\tau) = \frac{1}{2(N-2)\tau^2} \sum_{i=1}^{N-2} [x_{i+2} - 2x_{i+1} + x_i]^2, \quad (2.16)$$

where  $x_i$  is the  $i^{\text{th}}$  of the  $N = M + 1$  phase values spaced by the measurement interval  $\tau$ . Hence we have expressed the 2nd differences ( $z_i = \frac{y_{i+1} - y_i}{\tau}$ ) by inserting the elements ( $x_i$ ) of the 1st differences ( $\bar{y}_i = \frac{x_{i+1} - x_i}{\tau}$ ). So we compute the sum of the squares of these second differences for  $i = 1$  up to  $i = N - 2$  and then divide by  $2(N - 2)$ . Now we have what is called an estimate of the two-sample variance, AVAR. We divide by  $N - 2$  because that is the number of entries in the sum, and we divide by the factor 2 so that AVAR is equal to the classical variance in the case where all  $\bar{y}_i$  are random and uncorrelated [10]. The result is usually expressed as the square root  $\sigma_y(\tau)$ , the Allan deviation, ADEV. The confidence interval of an Allan deviation estimate is dependent on the noise type, but is often estimated as  $\pm\sigma_y(\tau)/\sqrt{N}$ . We see, that the longer the data length, the better is the confidence on the estimate.

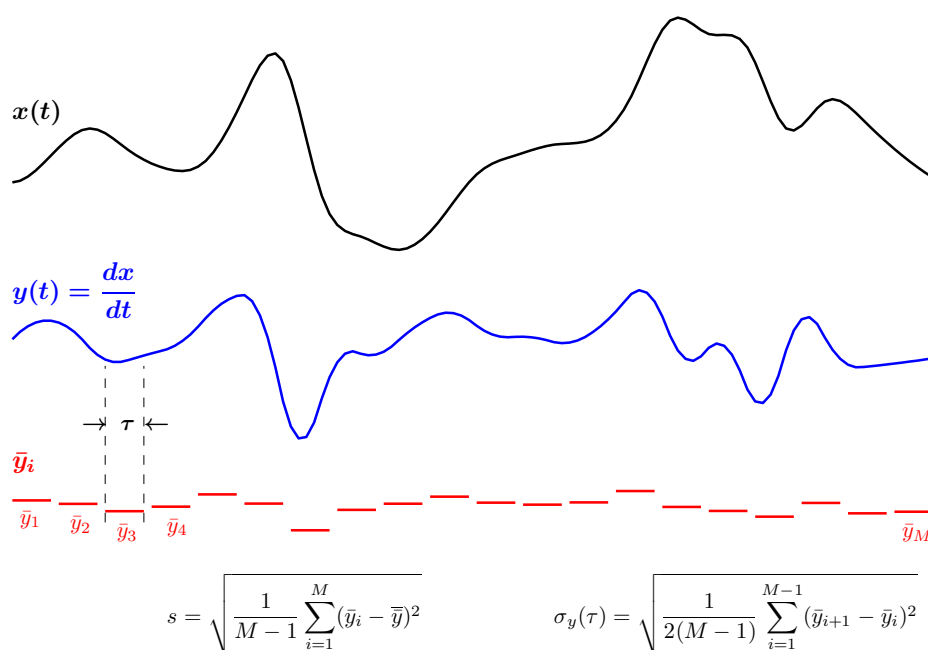


**Figure 2.2:** Simulated time deviation  $x(t)$  and fractional frequency plot  $y(t)$ .

Figure 2.2 shows a simulated time deviation plot  $x(t)$  (black) as well as a continuous fractional frequency plot  $y(t)$  below (blue), which indicates the slopes and derivations of  $x(t)$ . Beyond it, the sample time  $\tau$  is indicated over which each adjacent fractional frequency  $\bar{y}_i$  is averaged. Equations are for standard deviation and for estimate of  $\sigma_y(\tau)$  for finite data set of  $M$  frequency measurements  $\bar{y}_i$  (red). Often, standard deviation diverges as data length increases in measurement of long-term frequency stability of precision oscillators, whereas  $\sigma_y(\tau)$  converges [11, 12].

Note: Contrary to the common standard variance the distances to the mean of each value will be not computed, squared and summarized here. Allan replaced it by a summation over the squares of the distances of consecutive values. Further note that the original non-overlapping Allan variance has been largely superseded by its overlapping version.

### 2.2.3 Overlapping Allan Variance

Before presenting the formula of the overlapping Allan variance, the term *overlapping samples* shall be defined. Some stability calculations use overlapping samples, whereby the calculation is performed by utilizing all possible combinations of the data set, as shown in the figure below. The use of overlapping samples improves the confidence of the resulting stability estimate, but at the expense of greater computational time. The overlapping samples are not completely independent, but do increase the effective number of degrees of freedom. Overlapping samples do not apply at the basic measurement interval, which should be as short as practical to support a large number of overlaps at longer averaging times [4, 12].

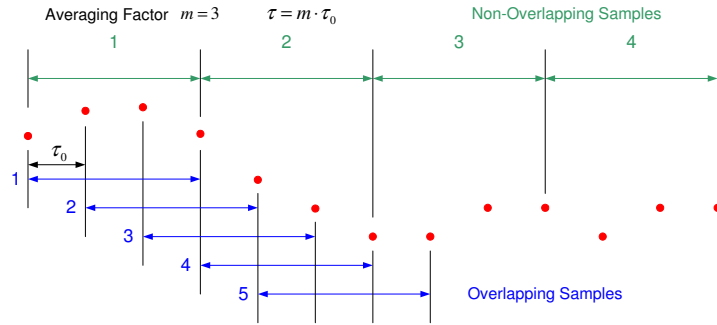


Figure 2.3: Comparison of non-overlapping and overlapping sampling

Figure 2.3 shows the different strides. For non-overlapped Allan variance the stride  $\tau$  is the averaging period and equals  $m \cdot \tau_0$ . In case of overlapped Allan variance the stride  $\tau_0$  equals the sample period. The fully overlapping Allan variance, also called AVAR, is accordingly a form of the normal Allan variance  $\sigma_y^2(\tau)$ , that makes maximum use of a data set by forming all possible overlapping samples at each averaging time  $\tau$ . It can be estimated from a set of  $M$  frequency measurements for averaging time  $\tau = m\tau_0$ , where  $m$  is the averaging factor and  $\tau_0$  is the basic measurement interval, by the expression

$$\sigma_y^2(\tau) = \frac{1}{2m^2(M-2m+1)} \sum_{j=1}^{M-2m+1} \left\{ \sum_{i=j}^{j+m-1} [\bar{y}_{i+m} - \bar{y}_i] \right\}^2. \quad (2.17)$$

In terms of phase data, the overlapping Allan variance can be estimated from a set of  $N = M + 1$  time measurements as

$$\sigma_y^2(\tau) = \frac{1}{2(N-2m)\tau^2} \sum_{i=1}^{N-2m} [x_{i+2m} - 2x_{i+m} + x_i]^2. \quad (2.18)$$

The argument of the sum can be written also as

$$[x_{i+2m} - 2x_{i+m} + x_i]^2 = [(x_{i+2m} - x_{i+m}) - (x_{i+m} - x_i)]^2 = [\bar{y}_{i+m} - \bar{y}_i]^2 \cdot \tau^2, \quad (2.19)$$

which is much clearer and easier to understand. Equation (2.17) and (2.18) can be transformed into each other as done in appendix A.

The result is usually expressed as the square root  $\sigma_y(\tau)$ , the Allan deviation ADEV. The confidence interval of an overlapping Allan deviation estimate is better than that of a normal Allan

variance estimation because, even though the additional overlapping differences are not all statistically independent, they nevertheless increase the number of degrees of freedom and thus improve the confidence in the estimation.

Note: The overlapping Allan deviation is the most common measure of time-domain frequency stability. The term AVAR has come to be used mainly for this form of the Allan variance, and ADEV for its square root.

**Derivation Model for the Overlapping Allan Variance**

$x$  samples

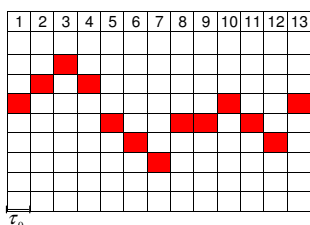
$$N = (M+1)$$

When only  $\bar{y}$  samples are given, the  $x$  samples can be obtained by integration:

$$x_n = \tau_0 \sum_{i=1}^{n-1} \bar{y}_i + C$$

where  $C$  is an integration constant.

$\bar{y}$  samples

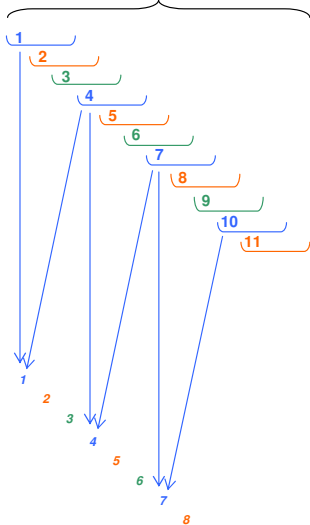


$M$

$$\bar{y}_i = 1/\tau_0 \cdot [x_{i+1} - x_i]$$

Averaging factor  $m$ , here:  $m = 3$

Averaging intervals,  $\tau = m \cdot \tau_0$



$M-m+1$

Averaged samples, averaged over  $m \cdot \tau_0$ . These averaged samples are designated as  $\bar{y}^{(\tau)}$

$$\bar{y}^{(\tau)}_i = \frac{1}{m\tau_0} [x_{i+m} - x_i]$$

$M-2m+1$  Sample Allan variances

$$\frac{1}{2} [\bar{y}^{(\tau)}_{i+m} - \bar{y}^{(\tau)}_i]^2$$

This model leads finally to

$$\sigma_y^2(m\tau_0) = \frac{1}{2m^2(M-2m+1)} \sum_{j=1}^{M-2m+1} \left\{ \sum_{i=j}^{j+m-1} [\bar{y}_{i+m} - \bar{y}_i] \right\}^2$$

$$= \frac{1}{2(N-2m)\tau^2} \sum_{i=1}^{N-2m} [x_{i+2m} - 2x_{i+m} + x_i]^2$$

as equation for the overlapping Allan variance.

Figure 2.4: Derivation model for the overlapping Allan variance

The two formulas depicted in the last box using frequency data  $\bar{y}$  and phase data  $x$  respectively can be transformed into each other (see appendix A).

### 2.2.4 Modified Allan Variance

The modified Allan variance  $Mod \sigma_y^2(\tau)$ , MVAR, is another common time domain measure of frequency stability [4, 9, 13, 14]. It is estimated from a set of  $M$  frequency measurements for averaging time  $\tau = m\tau_0$ , where  $m$  is the averaging factor and  $\tau_0$  is the basic measurement interval as is known, by the expression

$$Mod \sigma_y^2(\tau) = \frac{1}{2m^4(M-3m+2)} \sum_{j=1}^{M-3m+2} \left\{ \sum_{i=j}^{j+m-1} \left( \sum_{k=i}^{i+m-1} [\bar{y}_{k+m} - \bar{y}_k] \right) \right\}^2. \quad (2.20)$$

In terms of phase data, the modified Allan variance is estimated from a set of  $N = M + 1$  time measurements as

$$Mod \sigma_y^2(\tau) = \frac{1}{2m^2\tau^2(N-3m+1)} \sum_{j=1}^{N-3m+1} \left\{ \sum_{i=j}^{j+m-1} [x_{i+2m} - 2x_{i+m} + x_i] \right\}^2. \quad (2.21)$$

The result is usually expressed as the square root  $Mod \sigma_y(\tau)$ , the modified Allan deviation. The modified Allan variance is the same as the normal Allan variance for  $m = 1$ . It includes an additional phase averaging operation due to the inner loop. In other words, one first averages the phase data before performing the Allan deviation calculation. The modified Allan deviation has the advantage of being able to distinguish between white and flicker PM noise.

Note: Use the modified Allan deviation to distinguish between white and flicker PM noise. Modified Allan variance differs from basic Allan variance in the additional average over  $m$  adjacent measurements.

### 2.2.5 Overview of developed variances

The previous paragraphs introduced three types of Allan variances, but there exist many more. Different variances have been developed — actually arbitrarily — primarily to make best possible statements about stability of oscillators. These variances neither can be derived all together from one basic formula nor converted into each other. The often used measures non-overlapping, overlapping and modified Allan variances have been defined in the previous paragraphs. The Allan variance is the most common time domain measure of frequency stability, and as already mentioned there are several versions of it that provide better statistical confidence, can distinguish between white and flicker phase noise, and can describe time stability. The following table [4] is just for the sake of completeness and gives a review of all existing, as far as known by name variances used for stability analysis.

- All are second moment measures of dispersion - scatter or instability of frequency from central value.
- All are usually expressed as deviations.
- All are normalized to standard variance for white FM noise.

Variance Type	Characteristics
Standard	Non-convergent for some clock noises - don't use
Allan	Classic - use only if required - relatively poor confidence
Overlapping Allan	General purpose - most widely used - first choice
Modified Allan	Used to distinguish W and F PM
Time	Based on modified Allan variance
Hadamard	Rejects frequency drift, and handles divergent noise
Overlapping Hadamard	Better confidence than normal Hadamard
Total	Better confidence at long averages for Allan
Modified Total	Better confidence at long averages for modified Allan
Time Total	Better confidence at long averages for time
Hadamard Total	Better confidence at long averages for Hadamard
Thêo1	Provides information over nearly full record length
ThêoBR	Thêo1 with bias removed
ThêoH	Hybrid of Allan and ThêoBR variances

*Table 2.1: Overview of developed variances*

- All except standard variance converge for common clock noises.
- Modified types have additional phase averaging that can distinguish W and F PM noises.
- Time variances based on modified types.
- Hadamard types also converge for FW and RR FM noise.
- Overlapping types provide better confidence than classic Allan variance.
- Total types provide better confidence than corresponding overlapping types.
- ThêoH (hybrid-ThêoBR) and Thêo1 (Theoretical Variance #1) provide stability data out to 75% of record length.
- Some are quite computationally intensive, especially if results are wanted at all (or many) analysis intervals (averaging times)  $\tau$ . Use octave or decade  $\tau$  intervals.

## 2.3 The result of an Allan variance computation

Picking up again the introductory example already mentioned in chapter 1. Remember that the fictitious measuring device generates frequency values of the oscillator for each second. Assuming that the frequency signal of the oscillator would be affected by a superposed modulation of 0.5 Hz. No matter how small the part of the modulation is, it can always be detected by means of the one-second values, because a high-grade periodical up and down of the values can be noticed as shown in figure 2.5. The periodical up and down causes during computation of the Allan deviation (remember: the Allan deviation deals with consecutive values) that every single pair of values yields a nonzero part to the overall result (see black arrow in figure 2.5). The amount of the Allan deviation in this example depends on the travel of the modulation, but

is not relevant for this consideration. Important is that the superposed modulation is reflected in the Allan deviation for one-second values.

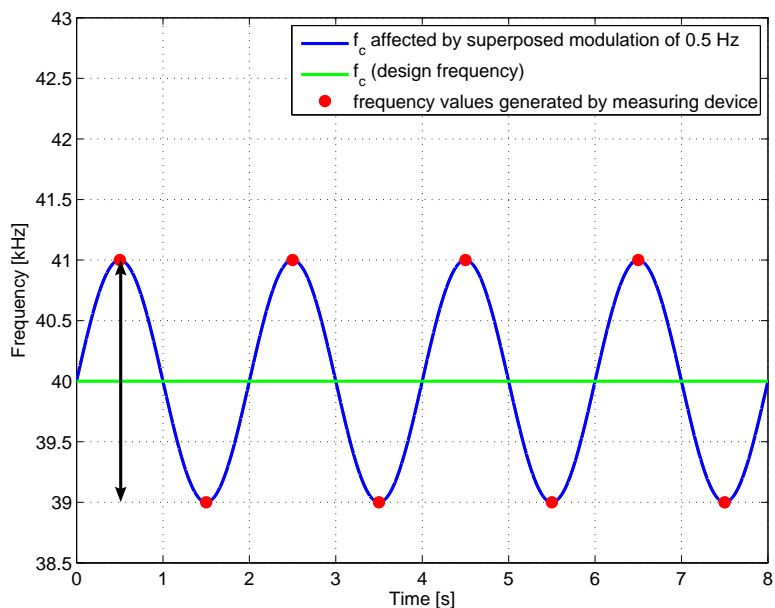


Figure 2.5: Frequency values of an oscillator in one-second cycles

If the measuring device generates frequency values of the oscillator only in two-second cycles (see figure 2.6) the gained data can be considered as a new time series. By two-second cycles received measurement values the superposed modulation could not be detected at all, because both the measurement values and the superposed modulation have the same period length. Hence the modulation is always caught at the same position of its period length.

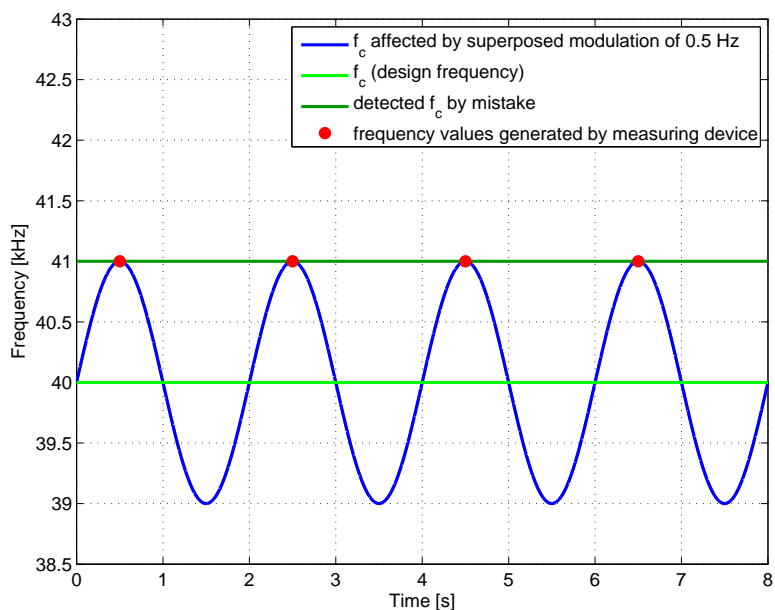


Figure 2.6: Frequency values of an oscillator in two-second cycles

Thus, one always measures the center frequency (denoted by  $f_c$  in figure 2.5 and 2.6) plus modulation at the same position and therefore a constant and incorrect frequency. But one recognizes absolutely nothing about the fact, that the superposed modulation entails a periodic change in oscillator frequency. Every pair of value would yield 0 as difference and finally an Allan deviation of 0, too. Consequently for two-second cycles one would mistake the oscillator for absolutely stable, although the oscillator is affected by a distinct superposed modulation and hence not stable at all.

By considering this introductory example two extremely important conclusions can be drawn:

- Firstly, the declaration of stability without any simultaneous information about the observation interval exactly for that stability is purposeless and useless. To make it clear, the observation interval is not the total testing time but the time interval between those measurement values used for computing the Allan deviation.
- Secondly, the computation of a single value of the Allan deviation is actually pointless, because a priori nobody knows at which frequencies an oscillator or different test item is affected by noise. Possibly important information about characteristics of a test item is kept back.

### 2.3.1 The Sigma-Tau-Diagram

Appropriate would be a presentation of the Allan deviation, from which for every reasonable observation interval the corresponding Allan deviation can be read out. Actually, there is such a presentation and it is the standard instrument in horology to characterize stability of oscillators. It is called sigma-tau diagram. The  $\sigma$  is the abbreviation of the Allan deviation and  $\tau$  is due to the fact, that in horology the observation interval is gladly represented by the Greek letter  $\tau$ . A sigma-tau-diagram evolves from many variance computations.

### 2.3.2 Comparison of three different Allan variance plots on the basis of a showcase data set

In the following, real frequency data of an oscillator from Agilent Technologies are analyzed by means of MATLAB files, that were developed in the course of this, and by using the  $\sigma$ - $\tau$ -diagram. The frequency data derive from a 10 MHz reference of an Agilent N9020A spectrum analyzer. An Agilent 3458A multimeter has been taken for measuring. Using this multimeter the frequency has been determined and recorded every 10 seconds. Figure 2.7 shows the plotted frequency data. The right plot includes the dimensionless fractional frequencies that are used for subsequent calculations.

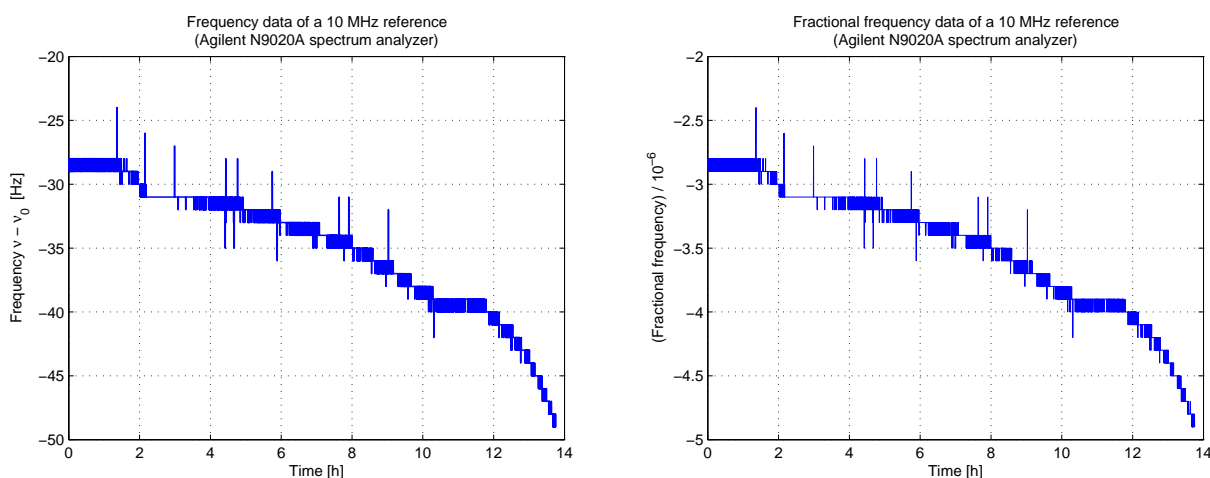


Figure 2.7: Frequency data of an oscillator

Due to several influences like pressure, temperature and aging, oscillators are not ideal and do not constantly resonate on the favored frequency (in this case 10 MHz). Now in order to answer the question "How stable is that oscillator?" one can compute the  $\sigma$ - $\tau$  diagram. On the basis of the frequency data, the three different diagrams of non-overlapping, overlapping and modified Allan deviation shall be shown. Figure 2.8 shows the result of non-overlapping ADEV computation, whereas figure 2.9 corresponds to overlapping ADEV, the first choice. Terminal figure 2.10 refers to modified Allan deviation.

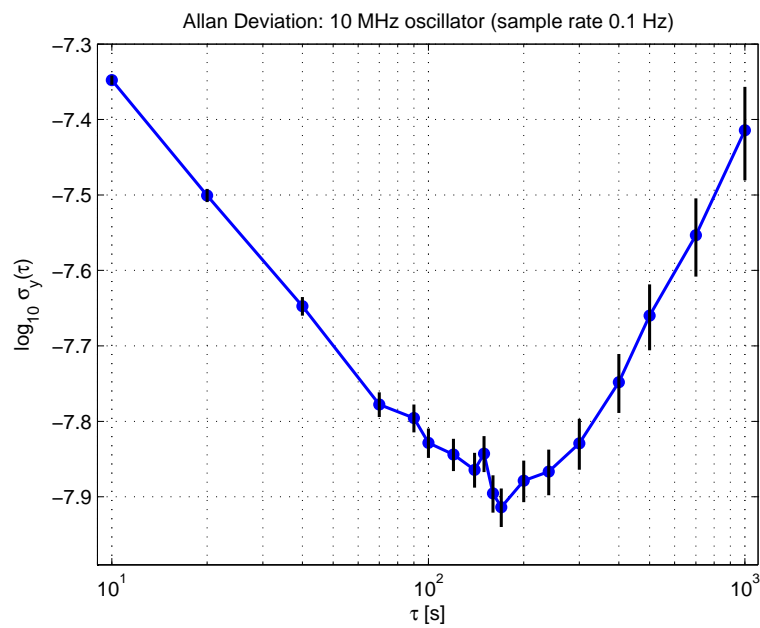


Figure 2.8:  $\sigma$ - $\tau$  diagram with non-overlapping Allan deviation on the basis of oscillator data

The blue dots demonstrate the chosen observation intervals. Additionally in each diagram black vertical error bars  $e_b$  are plotted, that augment with increasing averaging time  $\tau$ . The reason for that is the following: the larger my averaging time the less samples are left over. For that reason fewer and fewer values remain for computing Allan deviation and statistical uncertainty increases. One can clearly recognize it in figure 2.8 where overlapping intervals are not used.

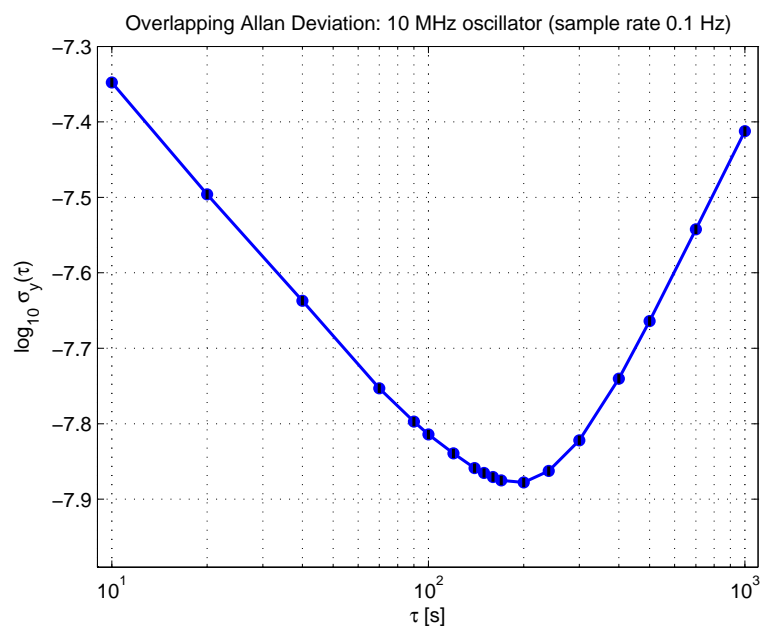


Figure 2.9:  $\sigma$ - $\tau$  diagram with overlapping Allan deviation on the basis of oscillator data

Considering figure 2.9 the augmentation of black error bars  $e_b$  is barely to detect. In addition, the curve is getting smoother, dithering vanishes. Overlapping Allan deviation utilizes all possible pairs of values, where co-partners exhibit the time interval  $\tau$ . That is why statistically more accurate conclusions than with simple Allan deviation can be made. One can see this fact by means of table 2.2.

Figure 2.9 demonstrates a boomerang-shaped curve, that is typical for oscillators. Until a specific averaging time  $\tau$  for this oscillator (i.e. here about 200 s) random processes prevail in the oscillator in consideration of its stability. Statistically, these random processes are of such a kind, that the larger the observation interval  $\tau$  the stronger the averaging out of these random processes. Thus, the stability will be improved.

Above 200 s the oscillator stability is obviously affected by processes, that cannot be averaged out with increasing observation time. Quite the contrary, they are becoming worse with increasing  $\tau$ . That is predominantly based on mentioned outside influences and aging.

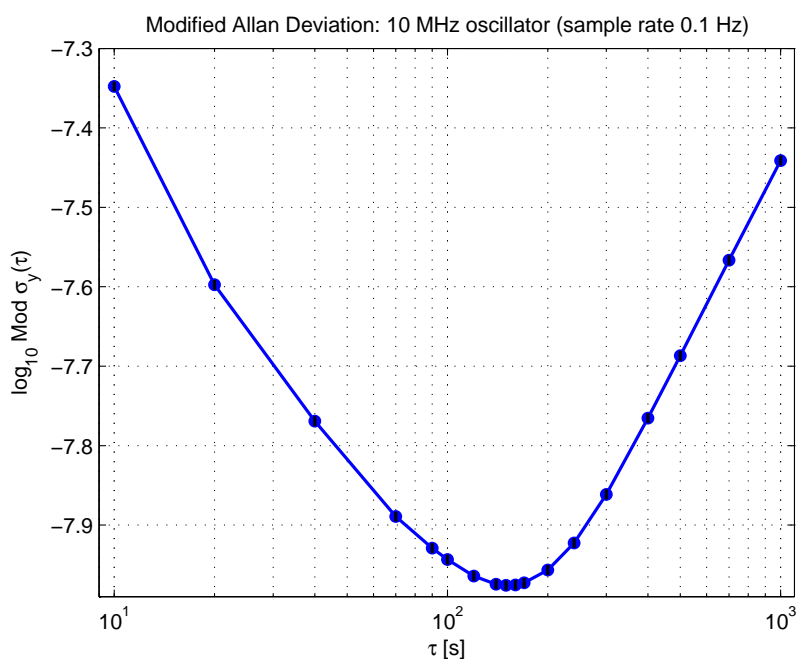


Figure 2.10:  $\sigma$ - $\tau$  diagram with modified Allan deviation on the basis of oscillator data

Figure 2.10 shows a smooth curve similar to the graphic with overlapping Allan deviation. In the corresponding column of table 2.2 as well as in the appropriate diagram one recognizes lower values, that are caused by the additional average over  $m$  adjacent measurements in  $\text{Mod } \sigma_y$  computation. As already mentioned the modified Allan deviation has its benefit to distinguish between white and flicker PM noise. Chapter 3.1 focuses on noise types.

$\tau$ [s]	Non-overlapping		Overlapping		Modified	
	$\sigma_y$ [ $10^{-8}$ ]	$e_b$ [ $10^{-9}$ ]	$\sigma_y$ [ $10^{-8}$ ]	$e_b$ [ $10^{-10}$ ]	$\sigma_y$ [ $10^{-8}$ ]	$e_b$ [ $10^{-10}$ ]
10	4.49	0.64	4.49	6.38	4.49	6.38
20	3.16	0.63	3.19	4.54	2.53	3.59
40	2.25	0.64	2.31	3.28	1.70	2.42
70	1.67	0.63	1.77	2.51	1.29	1.84
90	1.60	0.68	1.60	2.27	1.18	1.68
100	1.48	0.67	1.53	2.18	1.14	1.62
120	1.43	0.70	1.45	2.06	1.09	1.55
140	1.37	0.73	1.38	1.97	1.06	1.51
150	1.44	0.79	1.36	1.94	1.06	1.51
160	1.27	0.72	1.35	1.92	1.05	1.51
170	1.22	0.71	1.33	1.90	1.07	1.52
200	1.32	0.84	1.32	1.89	1.11	1.58
240	1.36	0.94	1.37	1.96	1.20	1.71
300	1.48	1.15	1.51	2.15	1.38	1.98
400	1.79	1.60	1.82	2.60	1.72	2.47
500	2.19	2.19	2.17	3.11	2.06	2.97
700	2.80	3.32	2.87	4.14	2.71	3.94
1000	3.85	5.45	3.87	5.61	3.62	5.31

*Table 2.2: Results of Allan deviation computation using oscillator frequency data*

Considering the result from overlapping ADEV computation, one arrives at the conclusion that the best stability is achieved at the reversal point of the curve. It is not possible to achieve a better one with that oscillator. If the oscillator is chosen as time basis in a frequency counter, a gate-time of 200s should be set. With that gate-time the most stable measurements can be gained. Even a further information is given by figure 2.9 or better by table 2.2 in the fact that one can expect a statistical error  $\sigma_y$  of  $1.3 \cdot 10^{-8}$  from measurement to measurement.

### 2.3.3 Computation times

Of course CPU times are dependent on length of input data and on numbers of  $\tau$ -values. In this case there are about 5000 measured data and 18  $\tau$ -values. This choice yields the following CPU times with MATLAB 7.1 on a normal PC:

	Non-overlapping	Overlapping	Modified
CPU times [s]	0.22	0.41	0.77

*Table 2.3: CPU times*

### 2.3.4 Accuracy versus Stability

This paragraph shall clarify that stable measurements are not necessarily accurate measurements. Stability and accuracy are two distinct qualities. If an oscillator does not resonate on nominal frequency, then it is an inaccurate one. However it can work on a wrong frequency stable at will. The difference between stability and accuracy is illustrated in figure 2.11.

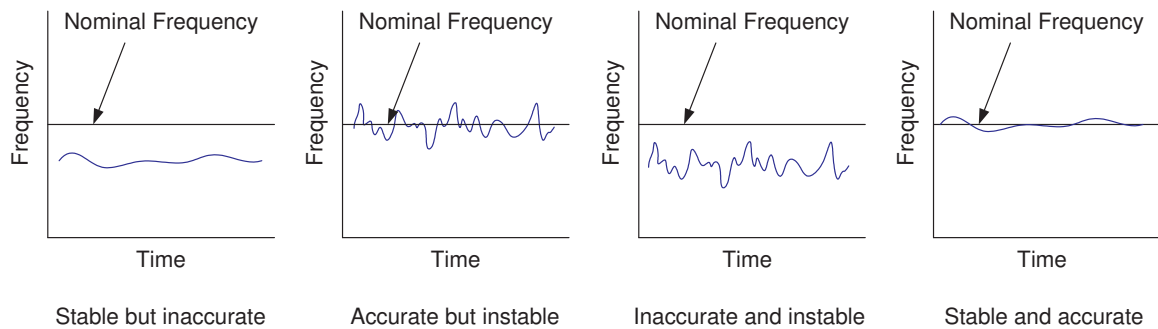


*Figure 2.11: Accuracy and stability are not the same!*

One would demand a standardized frequency to be accurate and stable as depicted far right in the sketch. If I want to employ the oscillator as time basis in a counter, there is no use for an accurate but instable standardized frequency as sketched in case 2. Arranging many measurements, they will be located around the correct value indeed, but I can trust a single measurement just as little as an inaccurate time basis. Hence for standardized frequencies accuracy has to be in reasonable relationship with stability [15].

## Chapter 3

# Frequency Domain Stability Analysis

Stability can also be characterized in the frequency domain in terms of a power spectral density (PSD) that describes the intensity of the phase or frequency fluctuations as a function of Fourier frequency. That is: The PSD describes the distribution in frequency of the power of a signal or a noise. Measured time series also underlie noise processes, that I want to examine more closely now.

### 3.1 Noise Spectra

The random phase and frequency fluctuations of a frequency source can be modeled by power law spectral densities of the form [4]

$$S_y(f) = h(\alpha) f^\alpha, \quad (3.1)$$

where

- $S_y(f)$  : One-sided power spectral density [1/Hz] of  $y$  with full power, in which  $y$  represents the fractional frequency fluctuations
- $f$  : Fourier or sideband frequency [Hz]
- $h(\alpha)$  : Intensity coefficient
- $\alpha$  : Exponent of the power law noise process.

Different noise types are listed in the following table, where PM means phase modulation and FM stands for frequency modulation.

Noise Type	$\alpha$
White PM	2
Flicker PM	1
White FM	0
Flicker FM	-1
Random Walk FM	-2
Flicker Walk FM	-3
Random Run FM	-4

*Table 3.1: Noise types with corresponding exponent*

The four most common of these noise types are White FM, Flicker FM, Random Walk FM and Flicker Walk FM. Noise type and time series for a set of simulated phase data are depicted in 3.1.

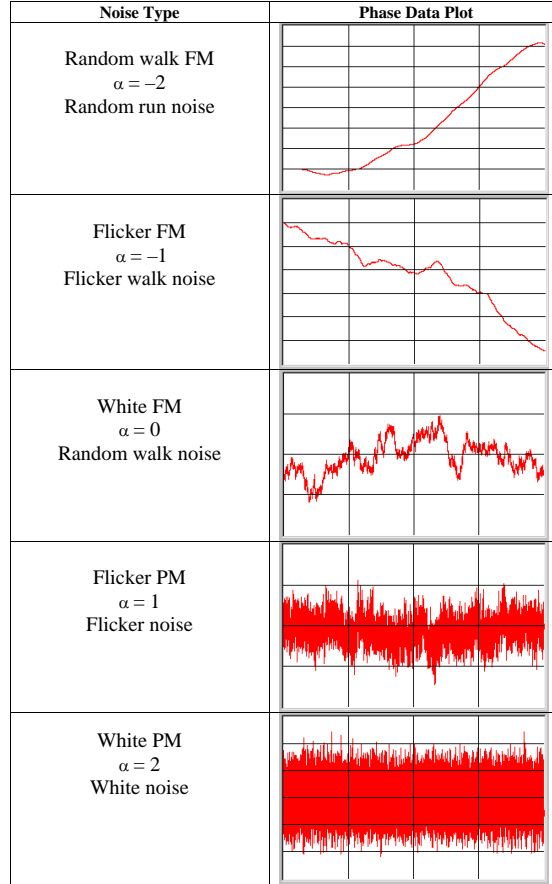


Figure 3.1: Noise type and time series for a set of simulated phase data.

Power law spectral models can be applied to both phase and frequency power spectral densities. Phase is the time integral of frequency, so the relationship between them varies as  $1/f^2$ .

$$S_x(f) = \frac{S_y(f)}{(2\pi f)^2}, \quad (3.2)$$

where  $S_x(f)$  is the PSD of the time fluctuations [ $s^2/\text{Hz}$ ].

Two other quantities are also commonly used to measure phase noise:

$S_\Phi(f)$ , the PSD of the phase fluctuations, [ $\text{rad}^2/\text{Hz}$ ] and its logarithmic equivalent  $\mathcal{L}(f)$ <sup>1</sup> [dBc/Hz]. The unit dBc/Hz is decibels relative to the carrier per Hertz. The relationship between these is

$$S_\Phi(f) = (2\pi\nu_0)^2 \cdot S_x(f) = \left(\frac{\nu_0}{f}\right)^2 \cdot S_y(f). \quad (3.3)$$

<sup>1</sup>

$\mathcal{L}(f) = 10 \cdot \log \left[ \frac{1}{2} \cdot S_\Phi(f) \right]$ , with positive frequencies and half power.

where  $\nu_0$  is the carrier frequency [Hz].

The power law exponent of the phase noise power spectral densities is  $\beta = \alpha - 2$ . These frequency domain power law exponents are also related to the slopes of the following time domain stability measures:

$$\begin{array}{lll} \text{Allan variance} & \sigma_y^2(\tau) & \mu = -(\alpha + 1), \alpha < 2 \\ \text{Modified Allan variance} & \text{Mod } \sigma_y^2(\tau) & \mu' = -(\alpha + 1), \alpha < 3 \end{array}$$

The spectral characteristics of the power law noise processes commonly used to describe the performance of frequency sources are shown in the following table.

Note, that  $\mu$  and  $\mu'$  are slopes and refer to Allan variances whereas a sigma tau diagram depicts Allan deviations with slopes  $\frac{\mu}{2}$  and  $\frac{\mu'}{2}$  respectively.

Noise Type	$\alpha$	$\beta$	$\mu$	$\mu'$
White PM	2	0	-2	-3
Flicker PM	1	-1	-2	-2
White FM	0	-2	-1	-1
Flicker FM	-1	-3	0	0
Random Walk FM	-2	-4	1	1

Table 3.2: Spectral characteristics of power law noise processes

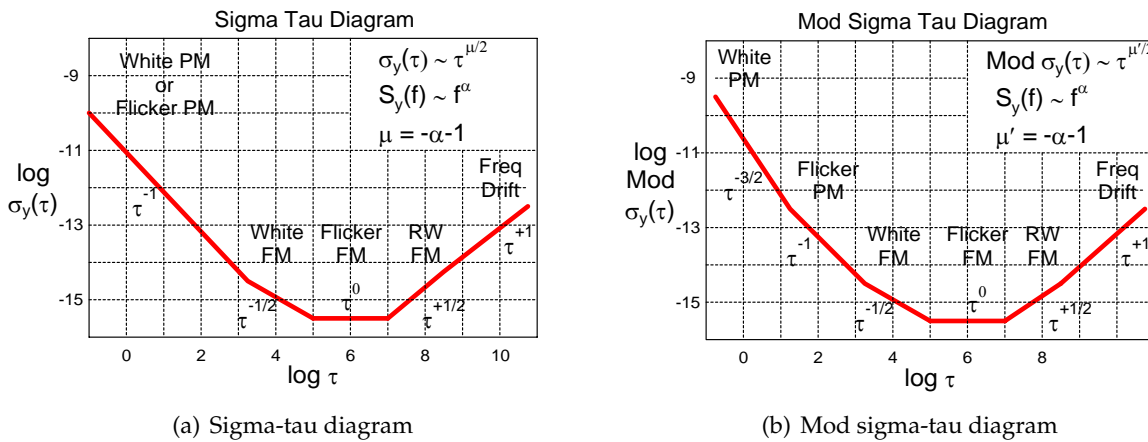


Figure 3.2: Slopes of common power law noise processes

Figure 3.2 depicts that on the basis of the slopes of sigma-tau diagrams one can identify the dominant power law noise process. It is often necessary to identify the dominant power law noise process of the spectral density of the fractional frequency fluctuations to perform a frequency stability analysis. Full particulars are obtainable in [16]. The most common method for power law noise identification is simply to observe the slope of a log-log plot of the Allan or modified Allan deviation versus averaging time, either manually or by fitting a line to it. Beyond there exist automatic calculation routines like the lag 1 autocorrelation method from W.J. Riley and C.A. Greenhall using a noise identification algorithm [16], but they are not yet fully developed up to now.

## 3.2 Spectral Analysis

Spectral Analysis is the process of characterizing the properties of a signal in the frequency domain, either as a power spectral density for noise, or as the amplitude and phase at discrete frequencies. Spectral Analysis can thus be applied to both noise and discrete components for frequency stability analysis. For the former, spectral analysis complements statistical analysis in the time domain. For the latter, spectral analysis can aid in the identification of periodic components such as interference and environmental sensitivity. Time domain data can be used to perform spectral analysis via the Fast Fourier Transform (FFT). The PSD can be computed corresponding to the Wiener-Chintschin-theorem [17]. Supposed a signal is given by a real-valued function  $x(t)$ , one can start from the autocorrelation function  $R_y(\tau)$

$$R_y(\tau) = \lim_{T \rightarrow \infty} \frac{1}{2T} \int_{-T}^T x(t) \cdot x(t + \tau) dt. \quad (3.4)$$

Now one defines the power spectral density  $S(f)$  of the function  $x(t)$  to be the Fourier transform of the autocorrelation function

$$S_y(f) = \int_{-\infty}^{\infty} R(\tau) \cdot e^{-j\omega\tau} d\tau \quad \omega = 2\pi f. \quad (3.5)$$

Or by using the Fourier integral

$$F_y(f) = \int_{-\infty}^{\infty} x(t) \cdot e^{-j2\pi ft} dt = |F_y| \cdot e^{j\Phi(f)} \quad (3.6)$$

where  $|F_y|$  is the amplitude spectrum and  $\Phi(f)$  represents the phase spectrum of the Fourier transform [18]. That yields as PSD

$$S_y(f) = |F_y|^2 = F_y \cdot F_y^*. \quad (3.7)$$

It is worthwhile noticing that under the assumption of Gaussian stationary random processes the power spectral density contains maximum information about the random process. The time-domain variances that will be defined in the next sections are related to the spectral density by some integral relationships, but do not include full characterization of the process [9]. Spectral analysis is most often used to characterize the short-term ( $< 1$  s) fluctuations of a frequency source, while a time domain analysis is most often used to provide information about the statistics of its instability over longer intervals ( $> 1$  s).

## 3.3 Domain Conversions

Now, the stability of a frequency source can be specified and measured in either the time domain or the frequency domain [4, 9, 19]. Examples of these stability measures are the Allan variance  $\sigma_y^2(\tau)$  in the time domain, and the spectral density of the fractional frequency fluctuations  $S_y(f)$  in the frequency domain. Conversions between these domains may be made by numerical integration of their fundamental relationship. The general conversion from time to frequency domain is not unique because white and flicker phase noise have the same Allan

variance dependence on  $\tau$ . Time domain frequency stability is related to the spectral density of the fractional frequency fluctuations by the relationship

$$\sigma_y^2(\tau) = \int_0^{\infty} S_y(f) \cdot |H(f)|^2 \cdot df, \quad (3.8)$$

where  $|H(f)|^2$  is the transfer function of the time domain sampling function. The transfer function of the Allan (two-sample) time domain stability is given by

$$|H(f)|^2 = 2 \left[ \frac{\sin^4(\pi\tau f)}{(\pi\tau f)^2} \right], \quad \text{with } 0 \leq f \leq f_h, \quad (3.9)$$

where  $f_h$  represents the maximum frequency of  $S_y(f)$ . Therefore the Allan variance can be found from the frequency domain by the expression

$$\sigma_y^2(\tau) = 2 \int_0^{f_h} S_y(f) \cdot \frac{\sin^4(\pi\tau f)}{(\pi\tau f)^2} df. \quad (3.10)$$

The equivalent expression for the modified Allan variance is

$$\text{Mod } \sigma_y^2(\tau) = \frac{2}{N^4 \pi^2 \tau_0^2} \int_0^{f_h} \frac{S_y(f) \sin^6(\pi\tau f)}{f^2 \sin^2(\pi\tau_0 f)} df \quad \text{with } \tau = N \cdot \tau_0. \quad (3.11)$$

There are no inversion formulas coming from Allan or modified Allan deviation to PSD. The only way for transformation would be to divide the sigma tau diagram into sections of equal slope and to work with few mathematical formulas or relationships that represent and describe common noise types. But usually one cannot act on the assumption that a given Allan variance process fits exactly to these basic mathematical descriptions of noise types. Hence this conversion is associated with a major loss of accuracy [20].

Exemplarily figure 3.3 depicts the transfer function of the Allan (two-sample) time domain stability.

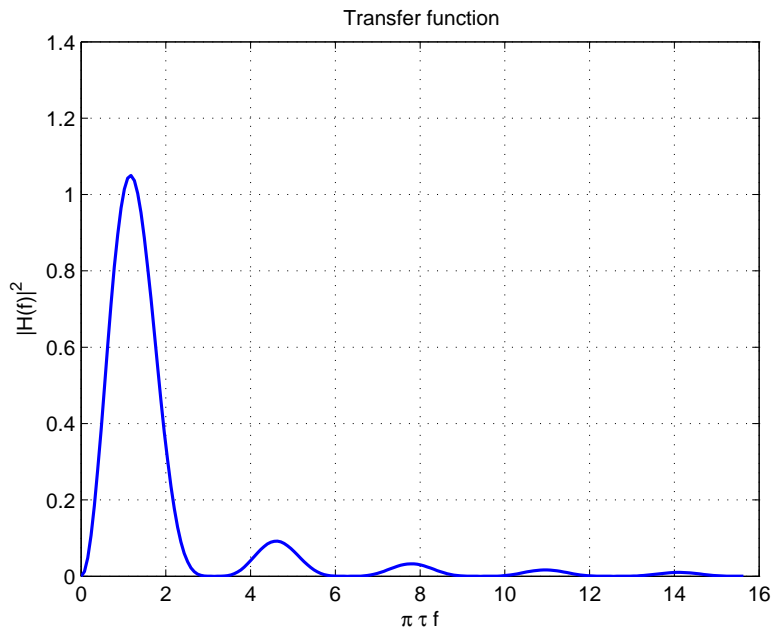
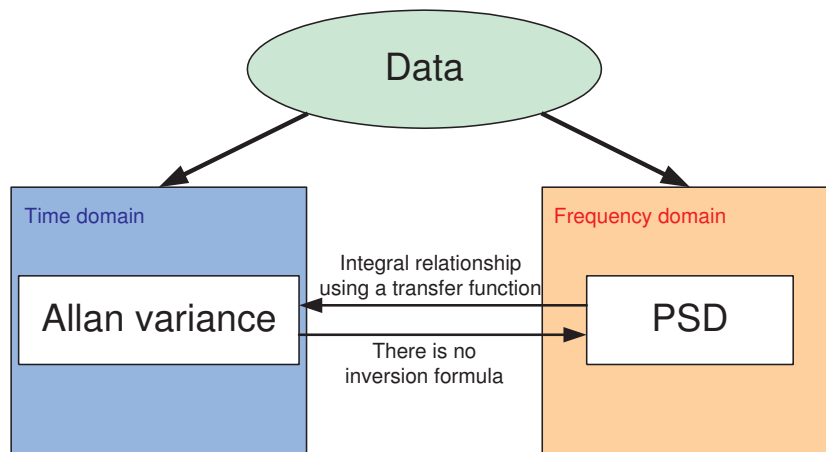


Figure 3.3: Transfer function of the Allan (two-sample) time domain stability

In summary, chapter 3 treated the basics for stability analysis in frequency domain, whereas chapter 2 focused on stability analysis in time domain. Furthermore, chapter 3 pointed out, that a direct conversion from PSD to Allan deviation is possible but not vice versa. This context is sketched in figure 3.4.



*Figure 3.4: Overview of domain conversions*

## Chapter 4

### Application to geodetic time series

The two central formulas (2.17) and (2.20) for direct Allan variance computation in time domain, i.e.

$$\sigma_y^2(\tau) = \frac{1}{2m^2(M-2m+1)} \sum_{j=1}^{M-2m+1} \left\{ \sum_{i=j}^{j+m-1} [\bar{y}_{i+m} - \bar{y}_i] \right\}^2$$

$$Mod \sigma_y^2(\tau) = \frac{1}{2m^4(M-3m+2)} \sum_{j=1}^{M-3m+2} \left\{ \sum_{i=j}^{j+m-1} \left( \sum_{k=i}^{i+m-1} [\bar{y}_{k+m} - \bar{y}_k] \right) \right\}^2$$

are now applied to geodetic time series. Subsequently sigma-tau diagrams are computed too by using the integral relationships (3.10) and (3.11) coming from frequency domain:

$$\sigma_y^2(\tau) = 2 \int_0^{f_h} S_y(f) \cdot \frac{\sin^4(\pi\tau f)}{(\pi\tau f)^2} df$$

$$Mod \sigma_y^2(\tau) = \frac{2}{N^4 \pi^2 \tau_0^2} \int_0^{f_h} \frac{S_y(f) \sin^6(\pi\tau f)}{f^2 \sin^2(\pi\tau_0 f)} df \quad \text{with } \tau = N \cdot \tau_0$$

Data types to be examined are:

- Oscillator frequencies
- Earth Orientation Parameters: Pole coordinates
- GPS measured coordinates
- Scintrex CG-5 Gravimeter data
- GOCE Gravity Gradients

Before starting with the application to the mentioned time series it is important to realize the following issue:

For geodetic time series (i.e. for all except oscillator frequencies in 4.1) the question arises, whether fractional frequency data as explained in equation 2.3 should be created or not. The answer is 'no', i.e. all examined geodetic time series are considered as  $\bar{y}$  data without reducing or normalizing by a nominal value. This implies that  $\bar{y}$  data are no longer dimensionless and that the calculated Allan deviations now include units.

## 4.1 Oscillator frequencies

As opening time series I start with a data set including oscillator frequencies. These data contain frequencies of a 10 MHz reference of an Agilent N9020A spectrum analyzer and have been recorded from Agilent Technologies<sup>1</sup> in Böblingen. For measurement an Agilent 3458A multi-meter has been used to detect and record the frequency every 10 seconds.

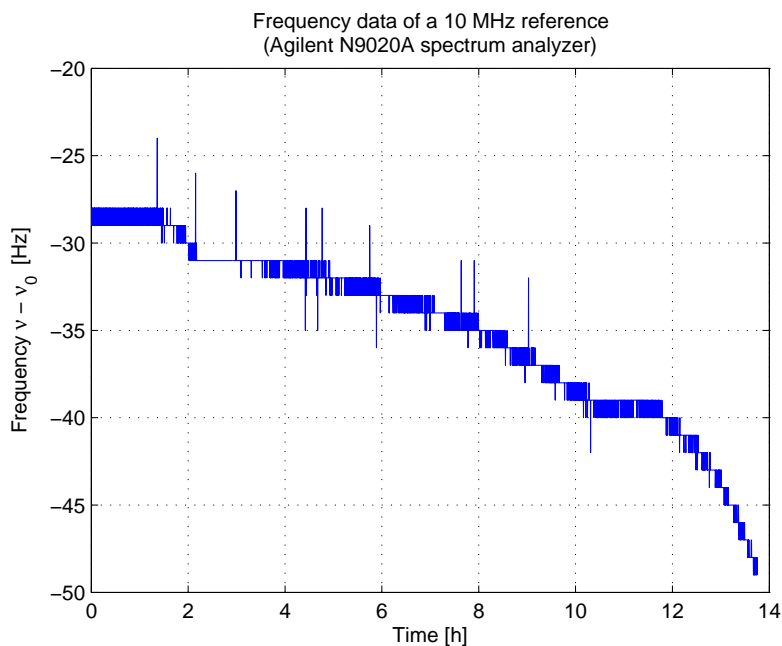


**Figure 4.1:** Frequency data of a 10 MHz reference of an Agilent N9020A spectrum analyzer

Figure 4.1 shows this data set. The frequencies  $\nu_i$  are reduced by the nominal frequency  $\nu_0 = 10$  MHz to achieve a better illustration.

It is noticeable that the frequency values neither start with nor achieve the nominal frequency 10 MHz, but even decline over time. Reasons therefor may be oscillator specific (like technical imperfection, aging) or due to environmental effects (temperature, pressure, humidity, dynamics).

<sup>1</sup>Data source: <http://www.home.agilent.com/agilent/home.jsp?lc=ger&cc=DE>

Hence, trend estimation of second order is made. Besides detrending only the first about 11 hours will be analyzed.

For  $\sigma$ - $\tau$ -diagram calculation fractional frequencies are used. That means that all recorded frequencies are reduced and normalized by its nominal frequency 10 MHz as described in equation 2.3.

The subsequent two figures 4.2 and 4.3 show  $\sigma$ - $\tau$ -plots for Allan deviation and modified Allan deviation respectively. Each figure includes two curves.

The blue curve is the result of Allan deviation computation in time domain using formulas (2.17) and (2.20) respectively.

The red one is the result of Allan deviation computation coming from frequency domain and using formulas (3.10) and (3.11) respectively with its corresponding transfer function and power spectral density.

The colored dots depict the computed Allan deviations at corresponding observation interval  $\tau$ . Both graphics (Allan deviation plot and modified Allan deviation plot) are always kept in equal co-domains for better possibility of comparison.

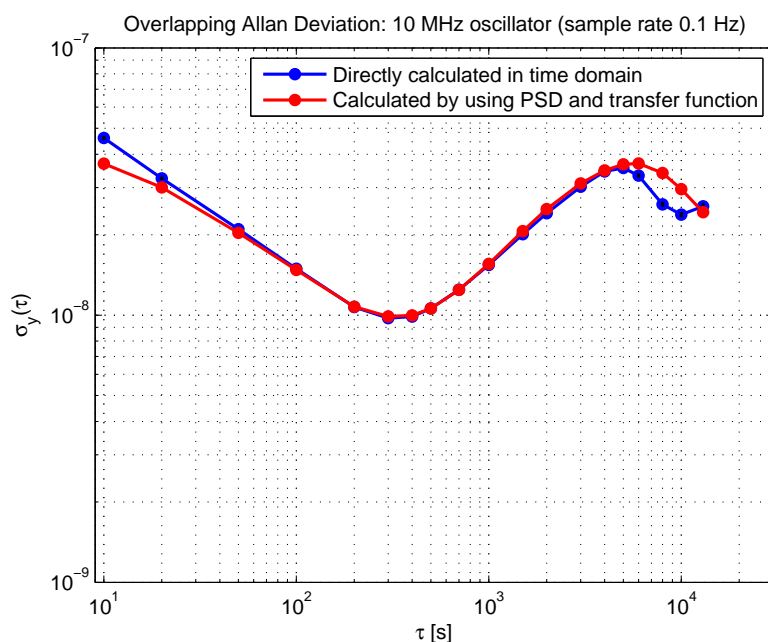


*Figure 4.2:  $\sigma$ - $\tau$ -diagram with Allan deviations for analyzed oscillator*

It is easily seen, that red and blue curve both fit together very well. Slight exceptions are only visible at the starting point and at the backmost area of the curve at  $\tau = 6000$  s and higher. But as already mentioned in chapter 2.3.2 backmost areas of an  $\sigma$ - $\tau$ -diagram may be negligible or at least should be read with caution because of increasing statistical uncertainty.

Figure 4.2 says that until averaging time  $\tau = 300$  s random processes prevail in the oscillator in consideration of its stability. The larger the observation interval  $\tau$ , the more these random processes are averaged out. Thus the stability will be improved.

Above 300 s the oscillator stability is obviously affected by processes, that cannot be averaged out with increasing observation time. Quite the contrary, they are becoming worse with increasing  $\tau$ .

One arrives at the conclusion that at the reversal point of the curve the best stability is achieved. It is not possible to achieve a better one with that oscillator. If the oscillator is chosen as time basis in a frequency counter, a gate-time of 300 s should be set. With that gate-time the most stable measurements can be gained. Here we can expect a statistical error from measurement to measurement of about  $10^{-8}$ .

It is also interesting to look at the numerical level of  $\sigma_y(\tau)$ . The worst stability is apparently obtained when using  $\tau = 10$  s as observation interval. Then a statistical error of about  $4 \cdot 10^{-8}$  is achieved.

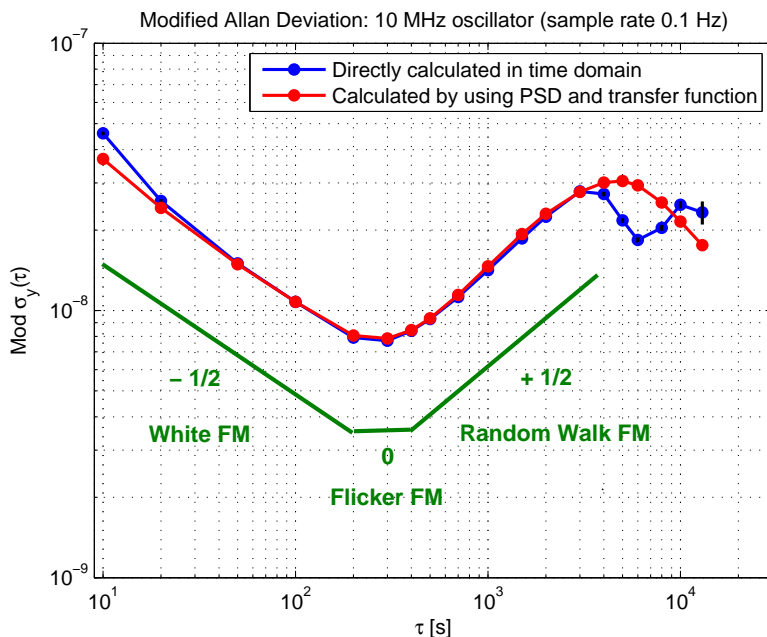


Figure 4.3:  $\sigma$ - $\tau$ -diagram with modified Allan deviations for analyzed oscillator

Figure 4.3 illustrates the  $\sigma$ - $\tau$ -diagram with modified Allan deviations. The curve progression points out a shape similar to the previous discussed  $\sigma$ - $\tau$ -diagram with overlapping Allan deviations. Remarkably, the results of modified Allan deviations turn out a bit lower in comparison with their corresponding overlapping Allan deviations. Keep in mind that the primary aim of the modified Allan deviations is just to point out distinctions between White and Flicker Phase Modulation noise as described in chapter 3.1. The most common method used in practice to distinguish between White and Flicker PM noise is to observe manually the slope of the log-log plot of the modified Allan deviation versus averaging time. The green lines symbolize this method in representing the slopes of the  $\sigma$ - $\tau$ -curves depicted in blue and red. Absolute values in the  $\sigma(\tau)$ -axis of these green lines have no significance.

Three different ranges are observed each with a specific slope. The first section up to about  $\tau = 200$  s can be estimated by a slope of  $-\frac{1}{2}$ , which means that up to an observation time  $\tau = 200$  s, this oscillator is affected by White FM (White frequency modulation). The second part with zero slope between  $\tau = 200$  s and  $\tau = 400$  s indicates Flicker FM. The last section with slope  $+\frac{1}{2}$  up to about  $\tau = 3000$  s is typical for Random Walk FM.

## 4.2 Earth Orientation Parameters: Pole coordinates

This section shall analyze earth orientation parameters, especially pole coordinates. Measurements of pole coordinates from International Earth Rotation and Reference Systems Service (IERS)<sup>2</sup> are taken as database. The chosen time series comprises data of pole coordinates from 1990 up to 2007 with one measurement per day.

As is known<sup>3</sup>, the pole underlies polar motion and is accurately described by  $x$  and  $y$ , which are the coordinates of the Celestial Ephemeris Pole (CEP) relative to the IRP, the IERS Reference Pole. The  $x$ -axis is in the direction of IRM, the IERS Reference Meridian; the  $y$ -axis is in the direction 90 degrees west longitude.

Polar motion consists of two quasi-periodic components and a gradual drift, mostly in the direction of the 80th meridian west, of the Earth's instantaneous rotational axis or North pole, from the conventionally defined reference axis.

The two periodic parts are a more or less circular motion. The one is called Chandler wobble with a period of about 435 days and is caused by the fact, that the earth rotation axis does not equal accurately the main axis of inertia. The other is a yearly circular motion and caused by seasonal mass shifting in atmosphere, by oceanic currents etc.

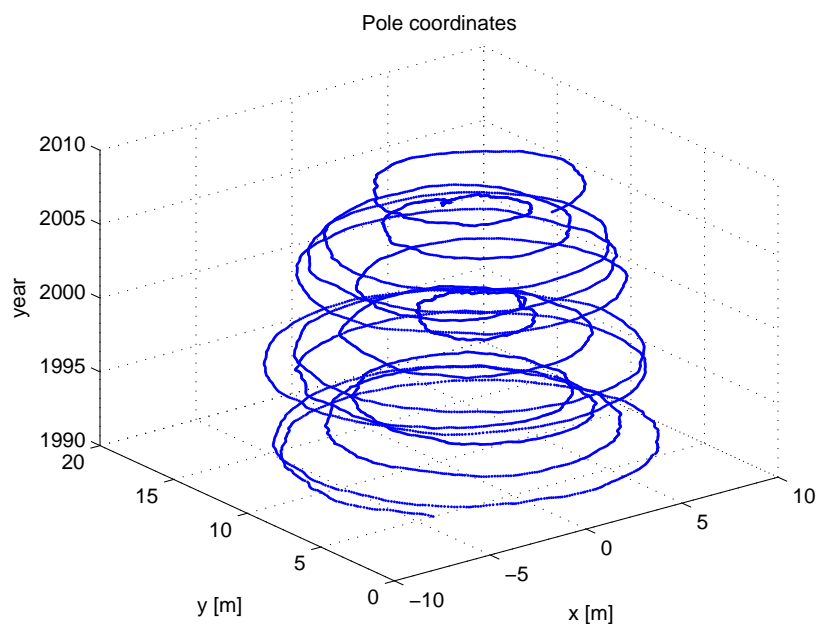


*Figure 4.4: Polar motion from 1990 up to 2007*

Figure 4.4 illustrates the polar motion over time. In further course this time series is separated into two data sets with exclusive  $x$ - and  $y$ -coordinates respectively. Although being conscious that both time series comprise periodic parts, no data preprocessing e.g. elimination of periodic content, is done this time. It begins with the  $x$ -coordinates.

<sup>2</sup>Data source: <http://www.iers.org>

<sup>3</sup>For more information see: [http://www.iers.org/nn\\_10910/IERS/EN/Science/EarthRotation/EOP.html?\\_\\_nnn=true](http://www.iers.org/nn_10910/IERS/EN/Science/EarthRotation/EOP.html?__nnn=true)

### 4.2.1 $x$ -component of pole coordinates

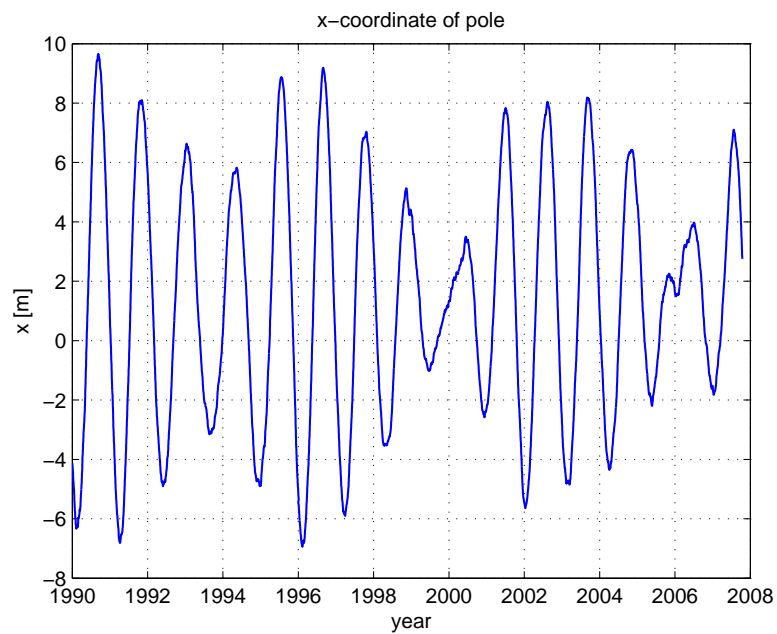


Figure 4.5:  $x$ -coordinate of pole from 1990 up to 2007

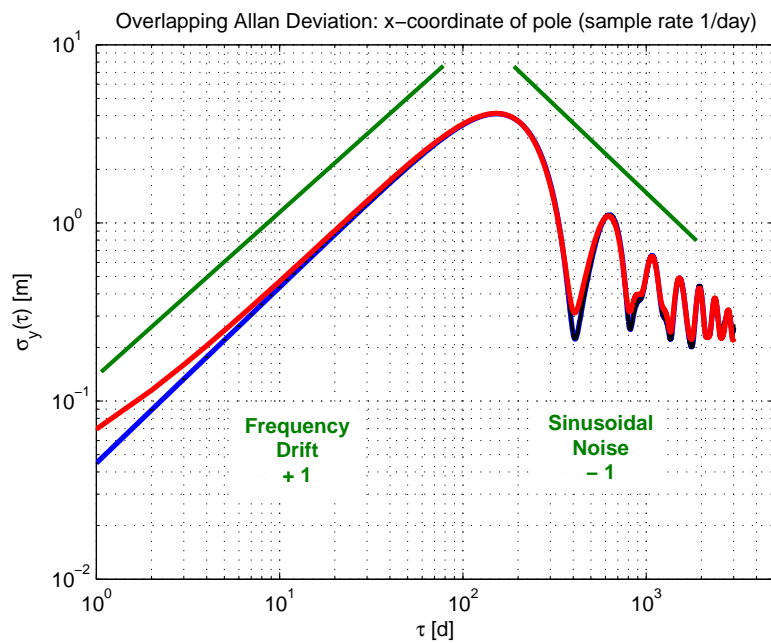


Figure 4.6:  $\sigma$ - $\tau$ -diagram with Allan deviations for  $x$ -coordinates of pole

The result of computation of Allan deviations is mainly shaped by an almost linear rise up to  $\sigma_y = 4$  m at about 150 days as observation interval  $\tau$ .

It is satisfying to see again both graphs fit well together (blue curve: directly calculated in the time domain; red curve: calculated by using the psd and a transfer function). This applies to both Allan deviation plot (Figure 4.6) and modified Allan deviation plot (Figure 4.7). The slopes are illustrated in figure 4.6 by green lines again. The predominating noise types are frequency drift and sinusoidal noise.

The linear rise is followed by decreasing sub-maxima with an envelope of slope -1, that represents the so-called sinusoidal noise. This noise type is explained in appendix B.

It is interesting to see that a local minimum occurs at about 400 days. Indeed, that is what one has to expect, because that is almost consistent with the Chandler wobble of about 435 days. A second minimum is visible at about 800 days, that is twice the Chandler period. For these  $\tau$ , as well as at further sub-minima for multiples of the Chandler period, the differences of adjacent values become very small in the ADEV calculation algorithm.

On the contrary, catching about the half period length (or odd multiples therefrom) of the mentioned Chandler wobble yields the highest instabilities with an absolute maximum of about  $\sigma_y = 4$  m. Here, the differences of adjacent values in the ADEV computation algorithm exhibit the biggest extent.

In strict sense, the absolute maximum of the curve does not exactly occur at the half period length of the Chandler wobble. This circumstance is explained in appendix B.

Hence, one can see that the periodicity of the time series is reflected again in the  $\sigma$ - $\tau$ -diagrams.

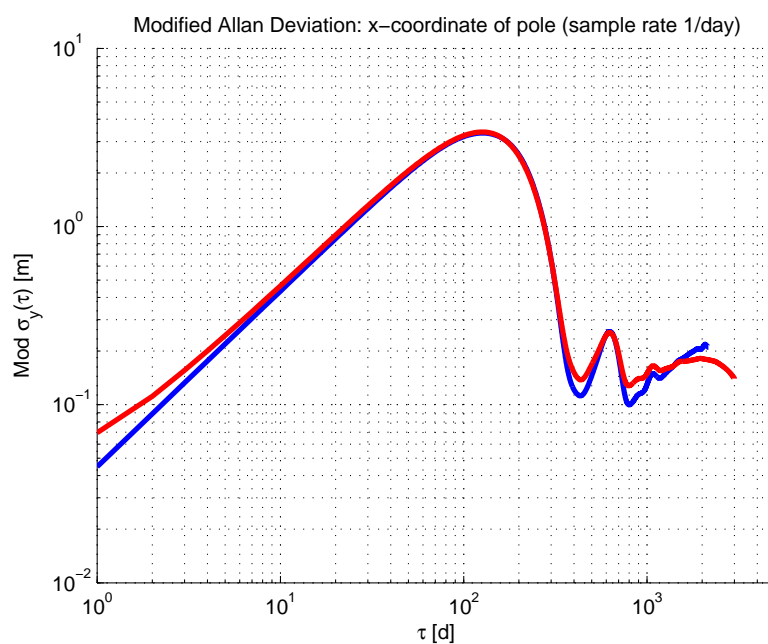


Figure 4.7:  $\sigma$ - $\tau$ -diagram with modified Allan deviations for x-coordinates of pole

### 4.2.2 $y$ -component of pole coordinates

Considering the co-partner of the pole coordinates one expects similar behaviour of the  $y$ -component. Not even the data plot but also both  $\sigma$ - $\tau$ -diagrams are of similar shape.

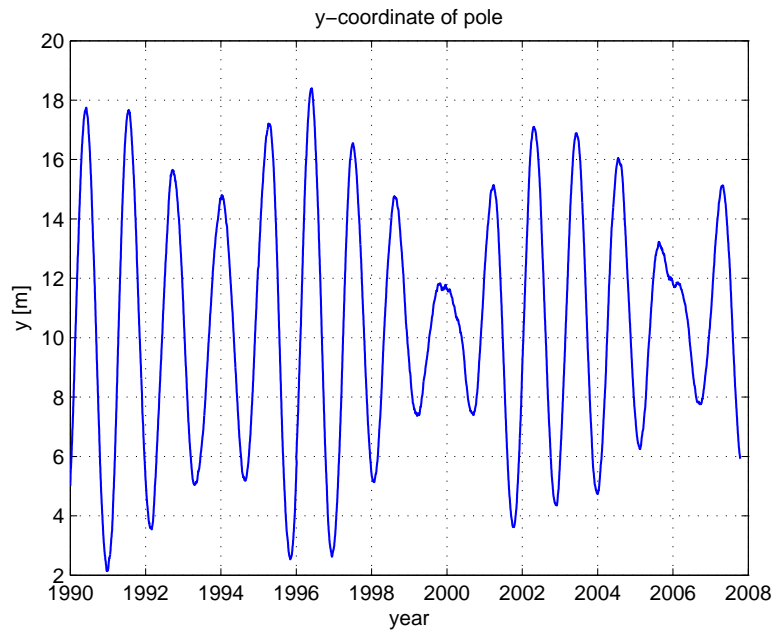


Figure 4.8:  $y$ -coordinate of pole from 1990 up to 2007

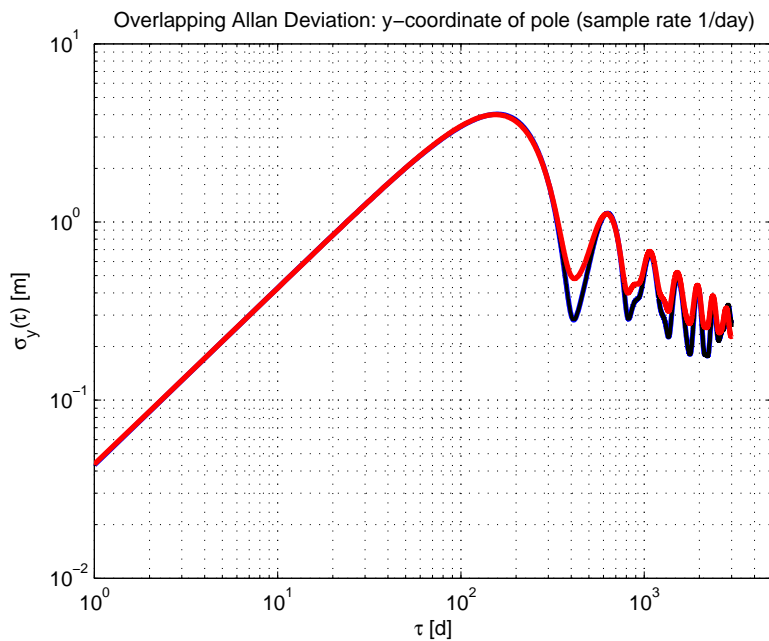


Figure 4.9:  $\sigma$ - $\tau$ -diagram with Allan deviations for  $y$ -coordinates of pole

Here, the same explanation and interpretation apply as for the x-component of the pole coordinates.

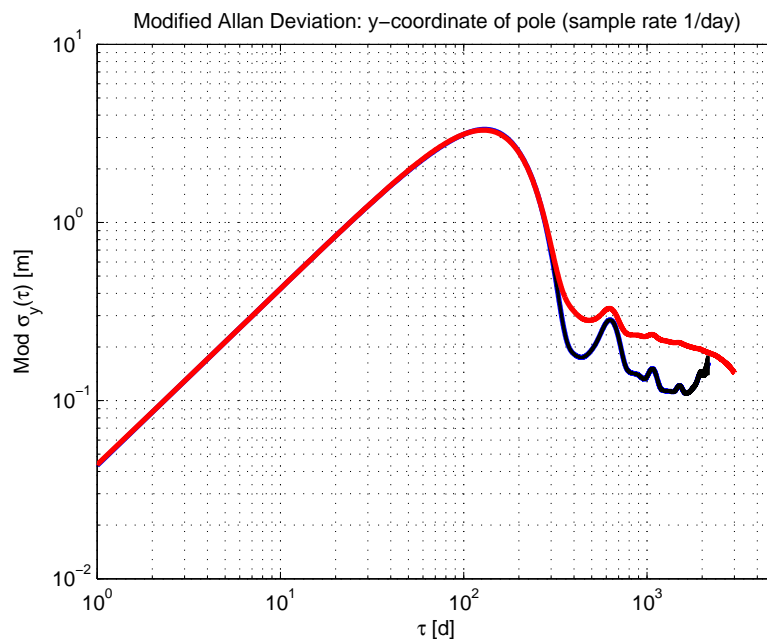


Figure 4.10:  $\sigma$ - $\tau$ -diagram with modified Allan deviations for y-coordinates of pole

### 4.3 GPS measured coordinates

Also GPS measurements can be used as a geodetic time series. For this purpose, position data have been measured with a data rate of 1 Hz over about 2.5 h, from a position with known coordinates, that is located at the Institute of Navigation (INS) of the University of Stuttgart<sup>4</sup>. More precisely, the data set is given as differential GPS (DGPS) positions with correction via EGNOS in National Marine Electronics Association (NMEA) format. The GPS-receiver used was a Trimble NetR8.

Having DGPS position data means that error sources like ephemeris error, satellite clock error, ionospheric and tropospheric refraction are removed. However the position data are still affected by run time error due to multipath effects, receiver clock error or variation of antenna phase center [21]. Hence this time series is not error-free.

So the data set comprises again position data for which all recorded coordinates have been transformed into a local system. Figure 4.11 illustrates this time series. Moreover, it is a good example to recognize the difference between stability and accuracy. The true position represented by the black cross is not located centrally within the scatter cloud. Therefore the measured position data are not accurate at all costs, but nevertheless they can reach a certain degree of stability.

<sup>4</sup>Data source: <http://www.nav.uni-stuttgart.de/>

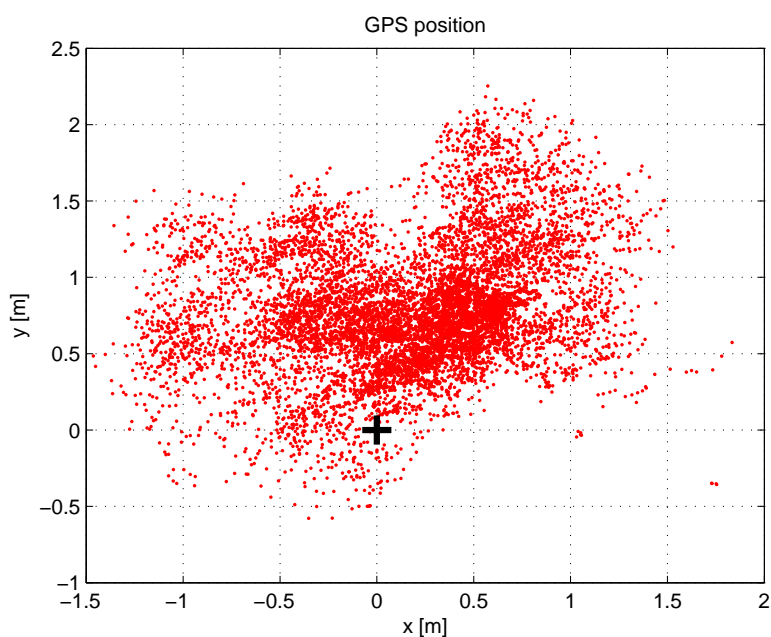


Figure 4.11: Scatter plot of GPS measured position data

In contrast to the previous data set of pole coordinates, the data here will be preprocessed differently — Just for the sake of choosing a different approach and point of view for position data. Since both horizontal components  $x$  and  $y$  belong together to a position in equal measure, it is physically more significant to incorporate both components. On top of that it represents a further method of treating two-dimensional data.

Therefore every measured position is considered as complex number, where the  $x$ -component presents the real part and the  $y$ -component the imaginary part.

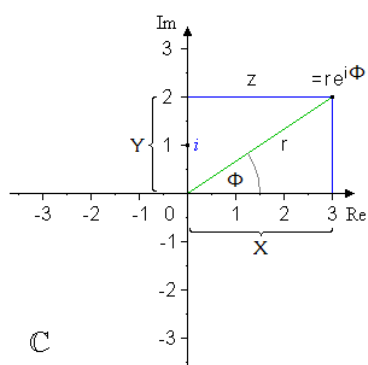


Figure 4.12: A complex number in the complex plane

Now, two time series can be created, namely one including absolute values  $r$  and another one with the arguments  $\phi$ :

$$z = x + yi$$

$$r = |z| = \sqrt{x^2 + y^2}$$

$$\phi = \arg(z)$$

Note that  $\sin \phi$  is computed for every argument of the complex GPS position data in order to avoid  $2\pi$  shifts between two points lying close together.

### 4.3.1 Absolute values of complex GPS position data

The time series with the absolute values attests, that all measured positions are located within a circle with radius 2.3 m around the true position.

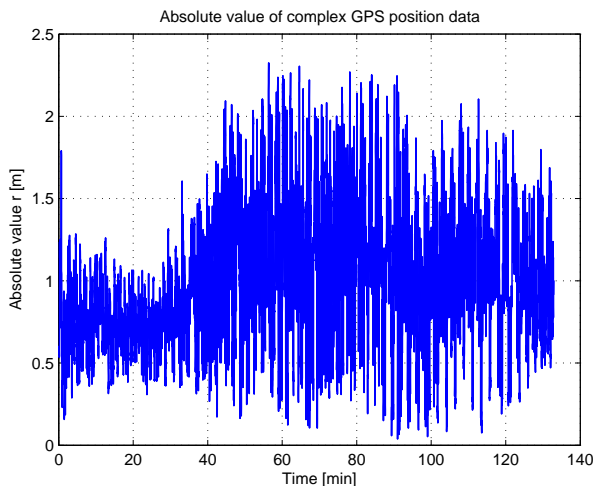


Figure 4.13: Time series with absolute values of complex GPS position data

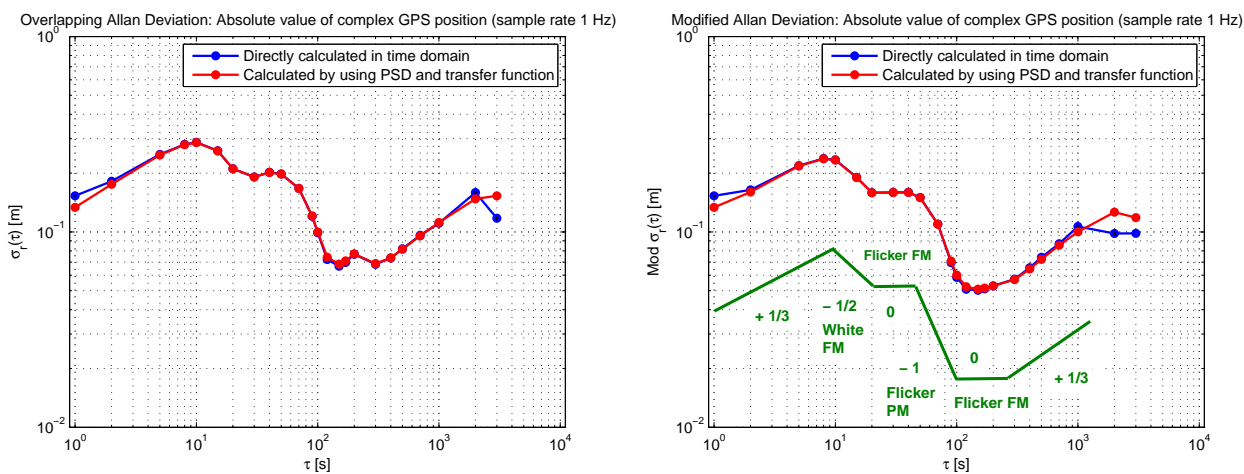


Figure 4.14:  $\sigma$ - $\tau$ -diagrams for absolute values

The codomain of the Allan deviations spans the range from 0.07 m to 0.30 m. The highest instability is obtained for  $\tau = 10$  s.

Within the range  $10 \text{ s} \leq \tau \leq 150 \text{ s}$  holds: The larger the observation interval, the stronger the filtering out of random processes with respect to the stability. Thus the stability becomes better and better with increasing  $\tau$  and reaches the optimum at the curve's minimum at 150 s with  $\sigma_r(\tau) \approx 6.7 \text{ cm}$ .

Apparently, above 150 s the stability of the absolute values of the GPS measurements depends on processes, that cannot be averaged out with increasing  $\tau$ , and thus degrades. By means of

figure 4.14 (right) some noise types are identified. There exist different ranges with different variance levels having zero slope and therefore uncover Flicker FM. Neither Random Walk FM (slope  $+\frac{1}{2}$ ) nor Flicker FM (slope 0) can be identified definitely at the beginning or the end of the diagram. These sections have slope  $+\frac{1}{3}$  and thus lie in between those noise types.

### 4.3.2 Arguments of complex GPS position data

The time series plot of the arguments include angles between  $\sin\left(\frac{\pi}{2}\right) = +1$  and  $\sin\left(-\frac{\pi}{2}\right) = -1$  as expected.

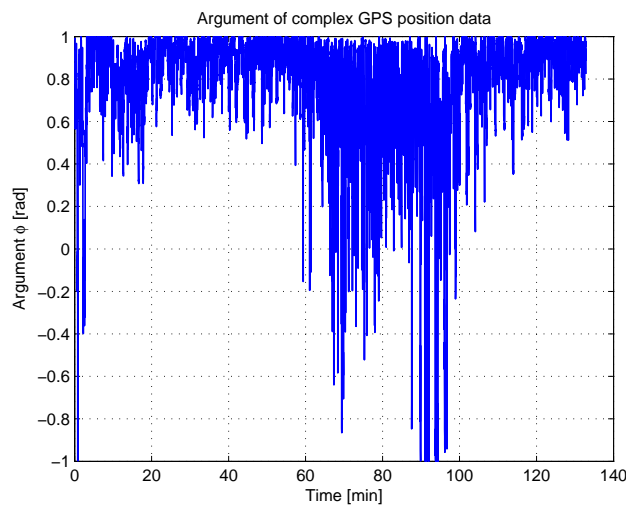


Figure 4.15: Time series with arguments of complex GPS position data

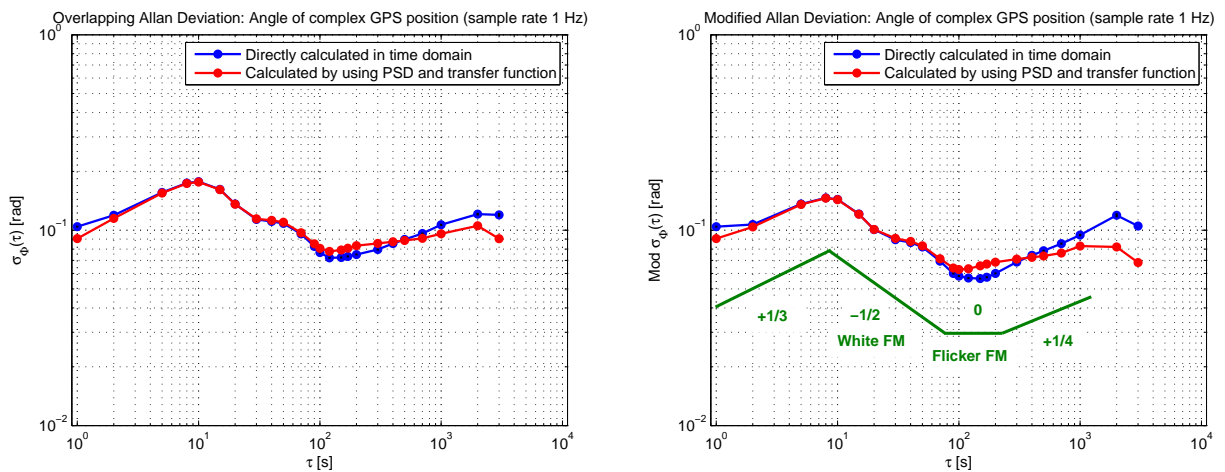


Figure 4.16:  $\sigma$ - $\tau$ -diagrams for arguments

The Allan deviations span the range from 0.07 rad to 0.18 rad. The highest instability lies at  $\tau = 10$  s again.

Figure 4.16 shows again: The larger the observation interval, the stronger random processes are filtered out with respect to the stability. For about 150 s one reaches its best value, i.e. 0.07 rad in case that one is interested in most stable measurements. Above 150 s the stability downgrades again.

With respect to the arguments the slopes are more coarse approximated as done before in the section with the absolute values. As a result of this fact ranges with Flicker FM and White FM are easily detected.

But in total it is difficult to detect clearly particular noise processes in this GPS positions data set.

## 4.4 Scintrex CG-5 Gravimeter data

The Scintrex CG-5 is a relative gravimeter and outputs relative gravity values. The device was located at the Institute of Geodesy at University of Stuttgart<sup>5</sup> for about two months and recorded one relative gravity value each minute. Hence the time series contains about 93000 data points in total.

Additionally it has to be pointed out that the data set is impaired by the effect of activated elevators in the institute building. Thus the data set is not flawless and vibration noise could not be minimized as desired [22].

The following figure illustrates this time series. For a better visualization, i.e. a better resolution in the vertical axis, the gravimeter data have been reduced by the mean value (left plot). In supplement, 3rd degree polynomial detrending was performed, in order to allow  $\sigma$ - $\tau$ -diagram computation. The result is depicted in Figure 4.17.

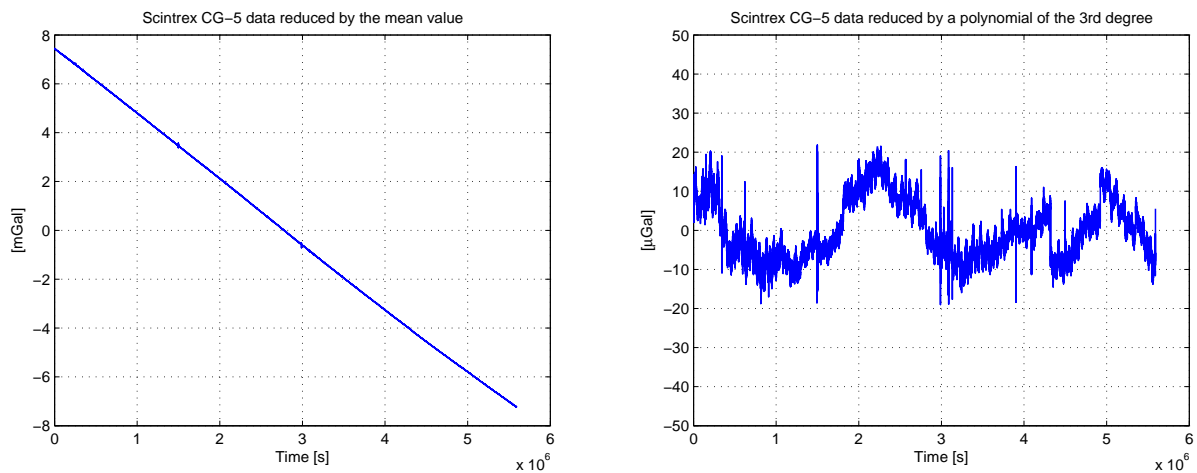


*Figure 4.17: Preprocessed gravimeter data*

The  $\sigma$ - $\tau$ -diagram in Figure 4.18 shows, that the most stable measurements are received at observation interval  $\tau = 1000$  s. This observation interval yields a stability of about  $0.5 \mu\text{Gal}$  from measure to measure. A second local minimum is detected at about  $\tau = 10 \text{ h} = 36000$  s. Here a

<sup>5</sup>Data source: <http://www.uni-stuttgart.de/gi/index.de.html>

stability of  $\sigma = 2 \mu\text{Gal}$  is achieved. The maximum and consequently most instable results are obtained with  $\tau \approx 11 \text{ d}$  ( $\sigma = 6 \mu\text{Gal}$ ).

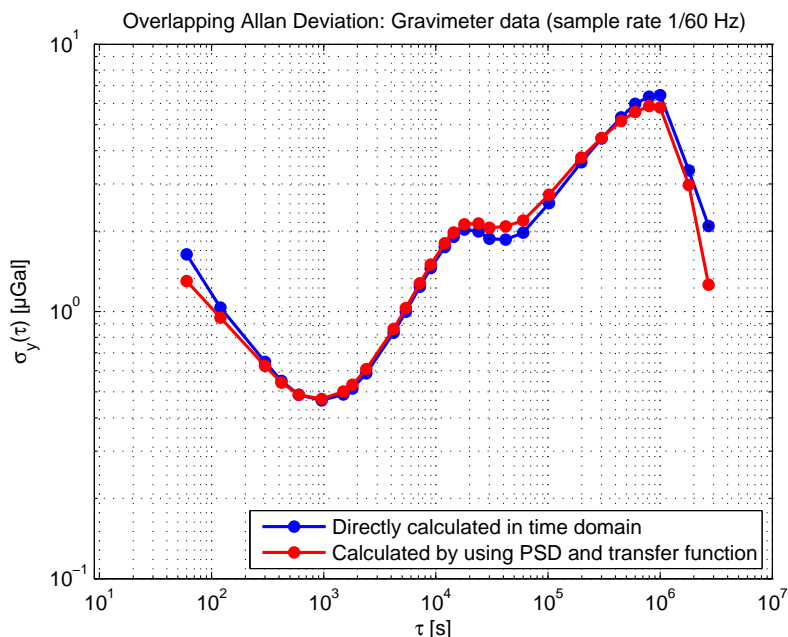


Figure 4.18:  $\sigma$ - $\tau$ -diagram with Allan deviations for gravimeter data

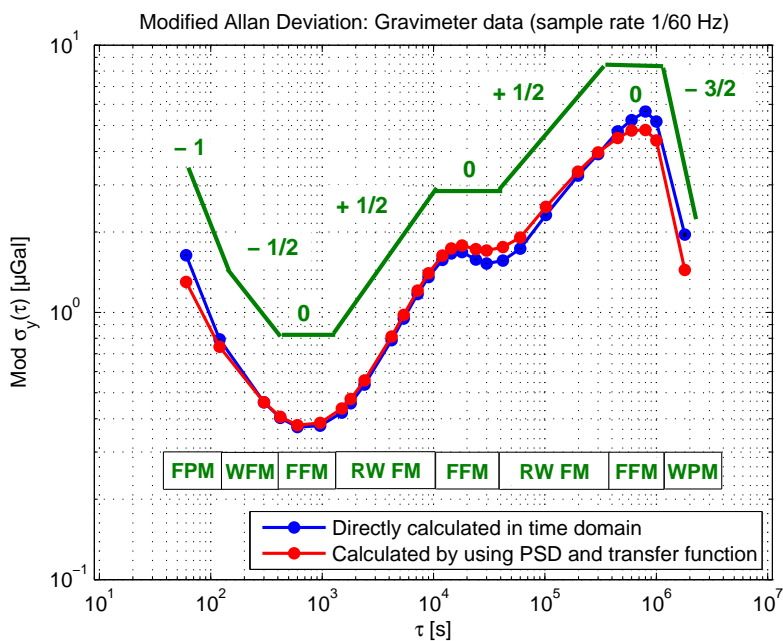


Figure 4.19:  $\sigma$ - $\tau$ -diagram with modified Allan deviations for gravimeter data

Figures 4.18 and 4.19 contain smooth  $\sigma$ - $\tau$ -diagrams regardless of which calculation method is used. In each case the result is a very interesting graph because it shows all power law noise

processes listed in table 3.2.

It seems to start with Flicker PM ( $60 \text{ s} \leq \tau \leq 150 \text{ s}$ ) and continues with a section of a nearly symmetric parabola. This parabola can be divided into three parts although being combined with smooth transitions:

White FM	:	$150 \text{ s} \leq \tau \leq 400 \text{ s}$
Flicker FM	:	$400 \text{ s} \leq \tau \leq 1200 \text{ s}$
Random Walk FM	:	$1200 \text{ s} \leq \tau \leq 10000 \text{ s}$

Subsequently, a range with zero slope is estimated before Random Walk FM is detected again. After a third section with Flicker FM at the graph's culmination, the last noise type of the five most common is identified: White PM for an averaging time  $\tau \geq 10^6 \text{ s}$ , i.e.  $\tau \geq 11 \text{ d}$ .

It is remarkable that wide ranges of the diagram are predominated by Flicker FM and Random Walk FM. Random Walk FM is believed to relate usually to the device's physical environment. Environmental effects like mechanical shock, vibration or temperature may cause such random shifts. Remember the previously mentioned activated elevators! These fit well into the quoted environmental effects.

Of course, it would have been interesting to keep the trend in the data. For this reason the ADEV calculation is caught up and compared with the one discussed before. Both sigma-tau curves are plotted in figure 4.20. The result is, that the trend changes enormously the shape of the curve. Almost an arising straight line is just left and further noise types can be detected barely besides the frequency drift. That is why detrending is necessary if one is interested in noise types detection. The idea is then to make the residuals after the deterministic drift removal as white as possible.

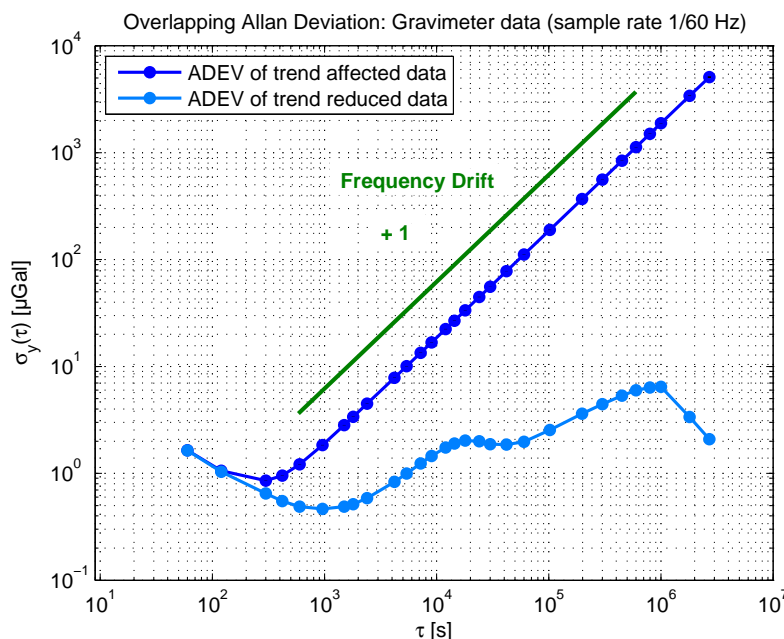


Figure 4.20: Difference in ADEV computation between trend reduced and trend affected data

## 4.5 GOCE gravity gradients

The last analyzed time series are gravity gradients measured by GOCE.

GOCE is the acronym for “Gravity field and steady-state Ocean Circulation Explorer mission”. The objective of GOCE is the determination of the stationary part of the Earth gravity field and geoid with highest possible spatial detail and accuracy.

The core instrument of GOCE is a three axis gravity gradiometer. It consists of three pairs of orthogonally mounted 3-axis accelerometers, i.e. an orthogonal arrangement of three one-axis gradiometers, with the x-axis nominally in the along track direction, the y-axis cross track and the z-axis roughly in the radial direction. The accelerometer in the radial direction is less sensitive than the others.

From the measured gravitational acceleration differences the three main diagonal terms of the gravitational tensor ( $T_{xx}$ ,  $T_{yy}$ ,  $T_{zz}$ ) as well as the off-diagonal term  $T_{xz}$  can be determined with high precision, whereas the off-diagonal terms  $T_{xy}$  and  $T_{yz}$  have a lower precision [23].

The tensor contains gravity gradients with units  $\frac{1}{s^2}$ . These units result from the derivative of the accelerations with respect to path  $\frac{da}{ds}$  with units  $\left[ \frac{\frac{m}{s^2}}{m} \right]$ :

$$T_{GOCE} = \begin{pmatrix} T_{xx} & T_{xy} & T_{xz} \\ T_{yx} & T_{yy} & T_{yz} \\ T_{zx} & T_{zy} & T_{zz} \end{pmatrix}$$

The analyzed time series consist of Level 2 data (EGG NOM 2)<sup>6</sup>, i.e. gravity gradients in the Gradiometer Reference Frame (GRF) corrected for temporal gravity field variations. Outliers and data gaps are identified and external calibration is applied. The sampling rate is 1 Hz, the total data length is 1 d = 86400 s. GOCE needs about 90 minutes for one revolution.

### 4.5.1 GOCE gravity gradients $T_{xx}$ , $T_{yy}$ and $T_{zz}$

First, the focus is on the three main diagonal terms ( $T_{xx}$ ,  $T_{yy}$ ,  $T_{zz}$ ) of the tensor beginning with  $T_{xx}$ .

The left graphic of Figure 4.21 depicts the  $T_{xx}$ -gradients in along track direction measured over one day. One recognizes a nearly periodic signal representing the almost 16 revolutions per day.

For stability analysis it is advised to detrend or to filter out periodic contents (that is like the removal of the reference field). Therefore the signal with  $T_{xx}$ -gradients is approximated by a Fourier series expansion. It is assumed that the gravity gradients  $T(t)$  compose of

$$T(t) = p(t) + n(t),$$

with a Fourier series  $p(t)$  and a noise component  $n(t)$ . The Fourier series expansion is carried out according to

$$p(t) = \frac{a_0}{2} + \sum_{k=1}^{\infty} (a_k \cdot \cos k\omega_0 t + b_k \cdot \sin k\omega_0 t)$$

<sup>6</sup>Data source: <http://www.uni-stuttgart.de/gi/index.de.html>

with coefficients

$$a_k = \frac{1}{\pi} \int_0^{2\pi} p(t) \cos k\omega_0 t dt \quad k = 0, 1, 2$$

$$b_k = \frac{1}{\pi} \int_0^{2\pi} p(t) \sin k\omega_0 t dt \quad k = 0, 1, 2$$

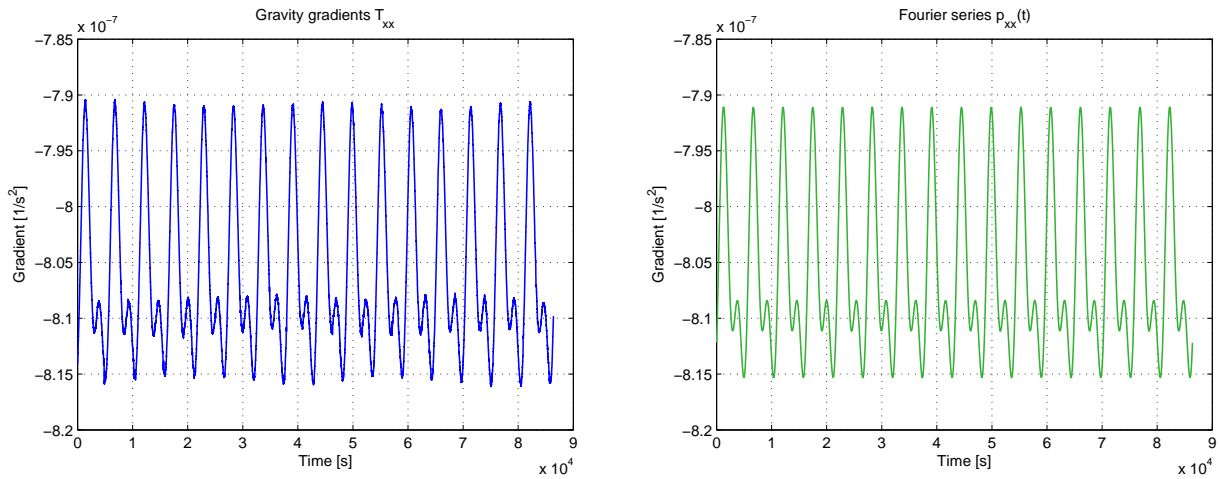


Figure 4.21: Gravity gradients in along track direction and an appropriate Fourier series

Hence most outstanding periodic contents are included in the Fourier series. By subtracting this Fourier series from the original gravity gradients time series one obtains the reduced gravity gradients  $T_{xx}$  (see Figure 4.22), that is  $n(t)$  in theory although being not exactly a pure noise signal.

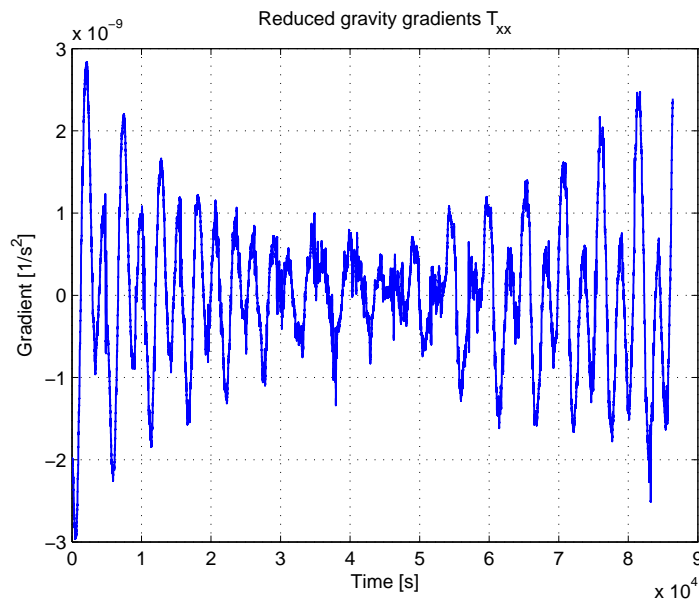


Figure 4.22: Reduced gravity gradients in along track direction

Figure 4.23 shows in summary, that this procedural method is chosen for all main diagonal terms of the tensor.

The known algorithms for Allan variance and modified Allan variance computation are applied to the reduced gravity gradients. As hitherto both versions (calculation in the time domain and via frequency domain) can be compared in Figure 4.24.

There all  $\sigma$ - $\tau$ -diagrams are shaped similarly and affected with an almost straight rise up to  $\tau = 1000$  s. The slope of this rise lies between  $\frac{\mu'}{2} = \frac{1}{2}$  and  $\frac{\mu'}{2} = 1$ . A unique noise identification is not feasible for this reason, but the rise generally says that periodic contents are still present.

In fact, a periodic content is obvious by means of the oscillations and beats considering the corresponding data plots of the reduced gravity gradients (Figure 4.23).

The range of the gravity gradients  $T_{zz}$  in radial direction turns out to be around twice as large as that of  $T_{xx}$  and  $T_{yy}$ . The signal of  $T_{zz}$  exhibits higher amplitudes than the signals of  $T_{xx}$  and  $T_{yy}$  (see Figure 4.23, last row). That is why the corresponding Allan deviations of  $T_{zz}$  generally represent an instability that is twice as high as in the  $\sigma$ - $\tau$ -plots of  $T_{xx}$  and  $T_{yy}$ .

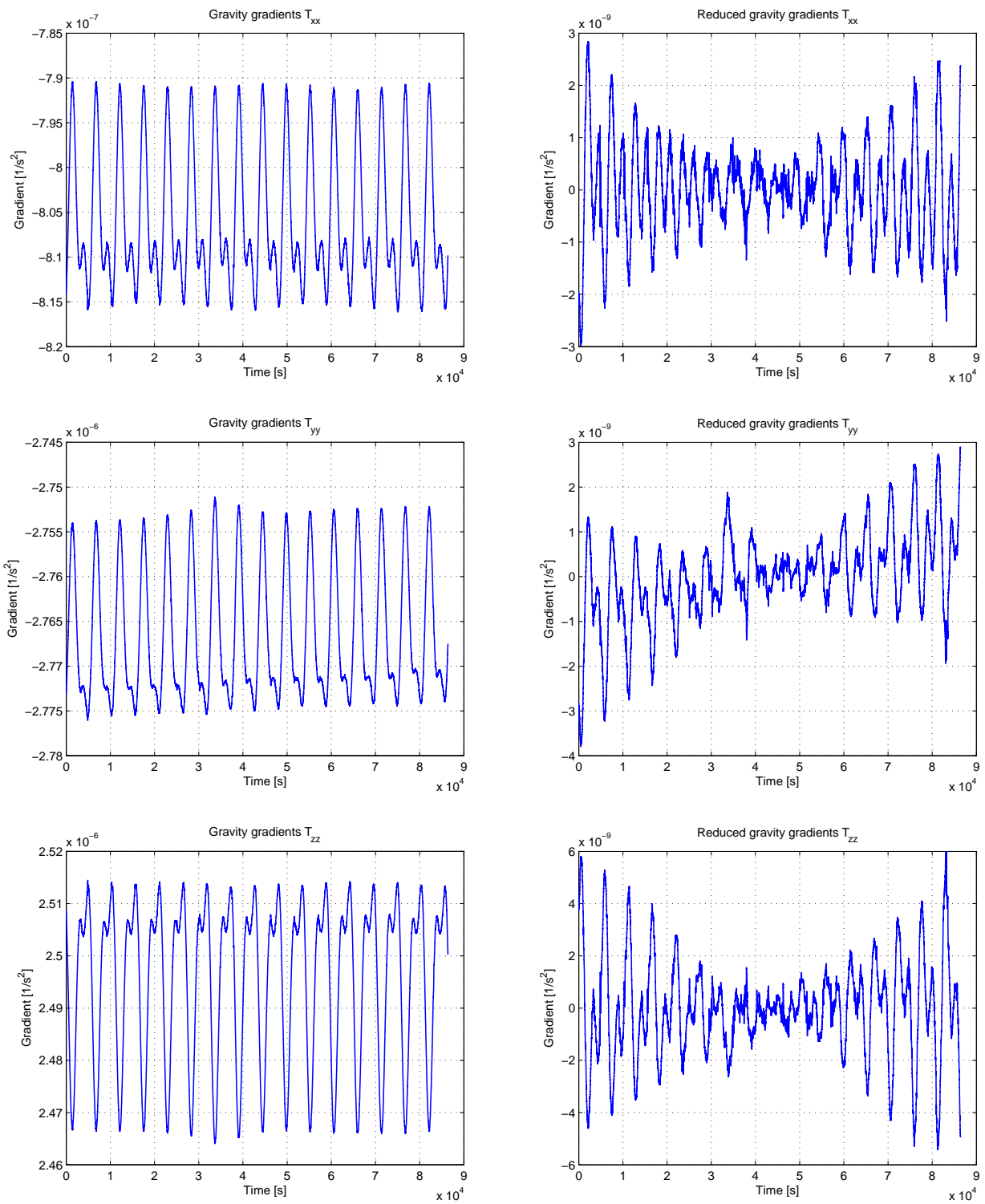


Figure 4.23: Original and reduced gravity gradients of the three main diagonal terms  $T_{xx}$ ,  $T_{yy}$  and  $T_{zz}$

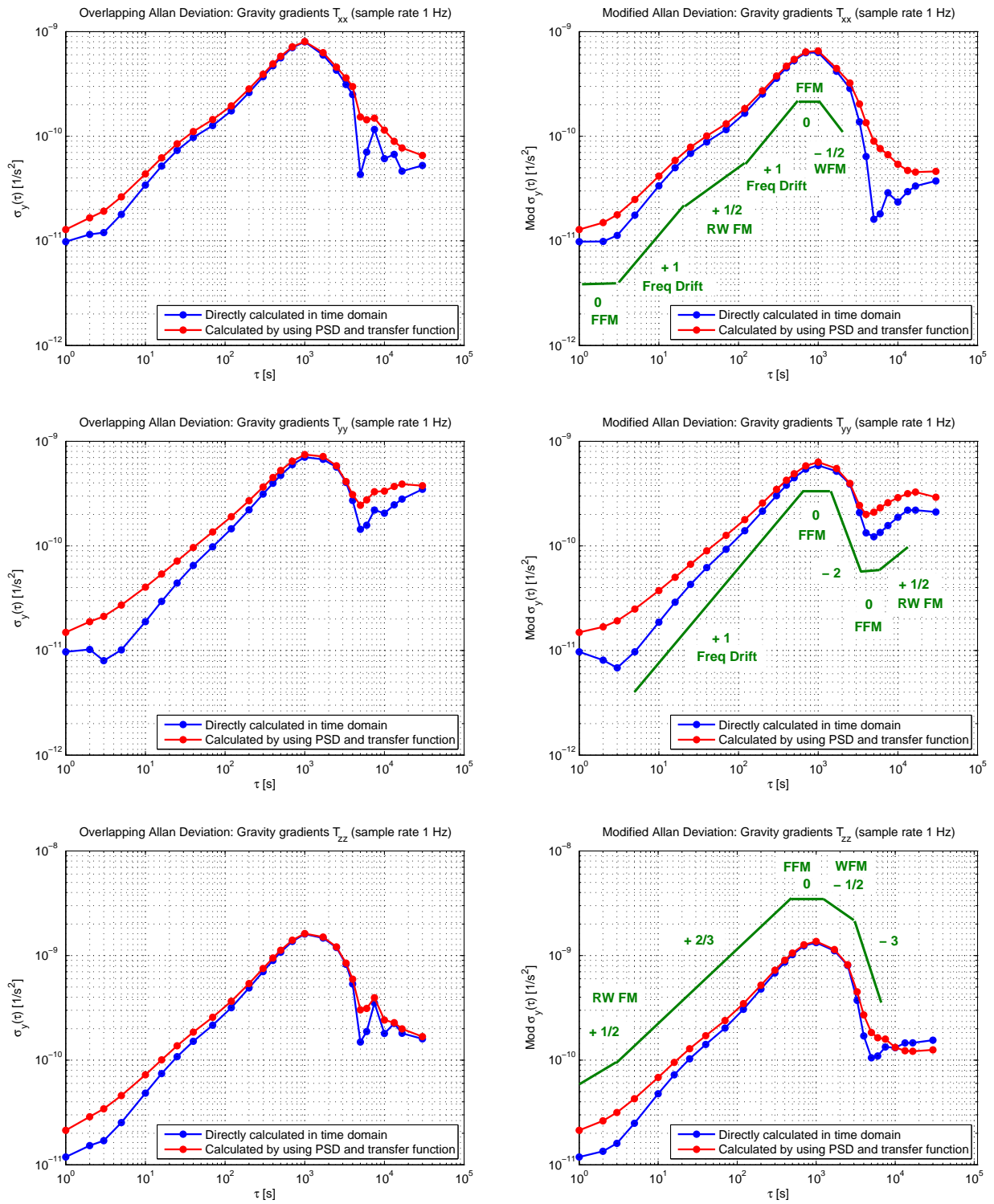


Figure 4.24:  $\sigma$ - $\tau$ -diagrams of the three main diagonal terms  $T_{xx}$ ,  $T_{yy}$  and  $T_{zz}$

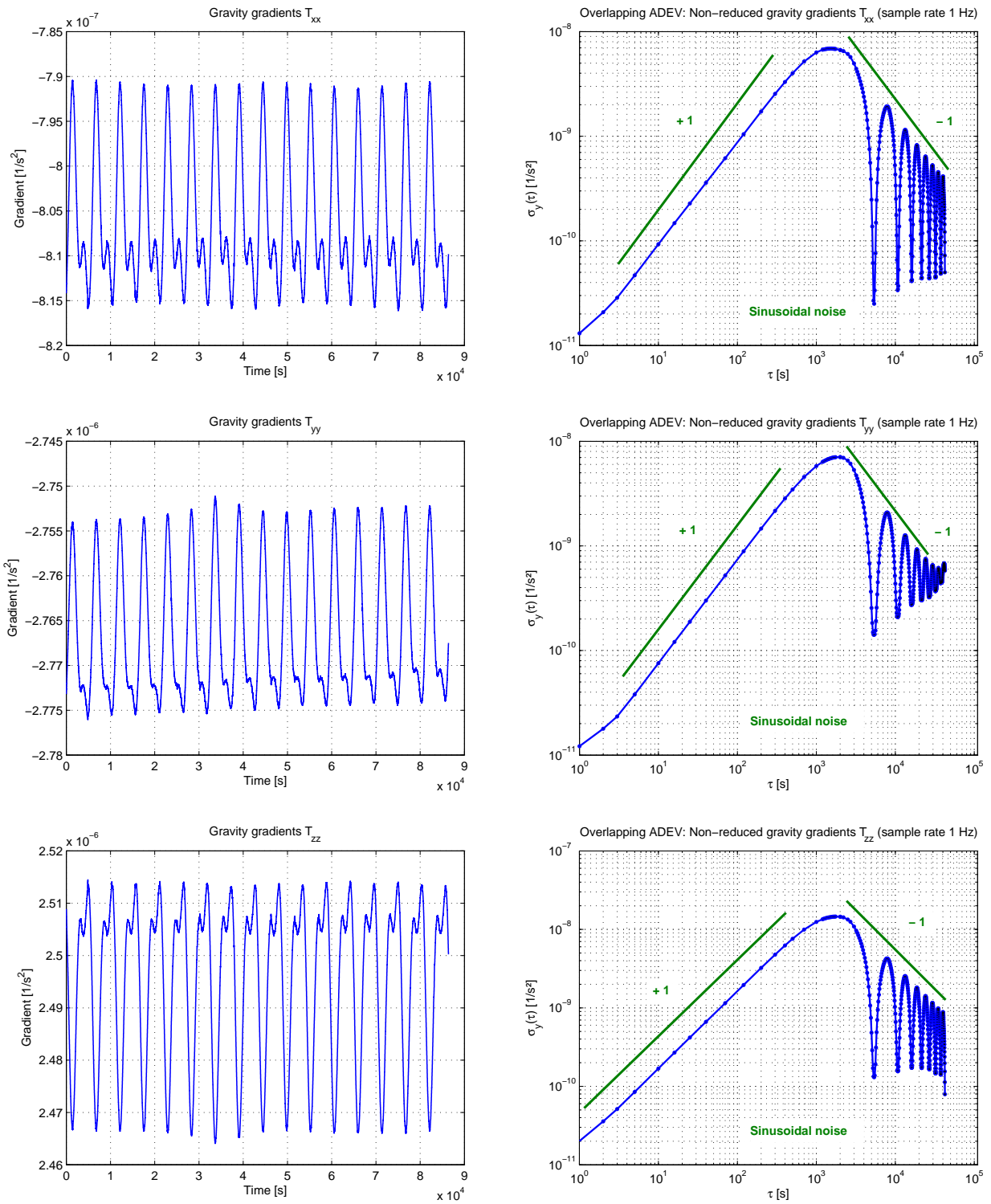


Figure 4.25: Original gravity gradients of the three main diagonal terms  $T_{xx}$ ,  $T_{yy}$ ,  $T_{zz}$  and their corresponding time-domain based sigma-tau plots

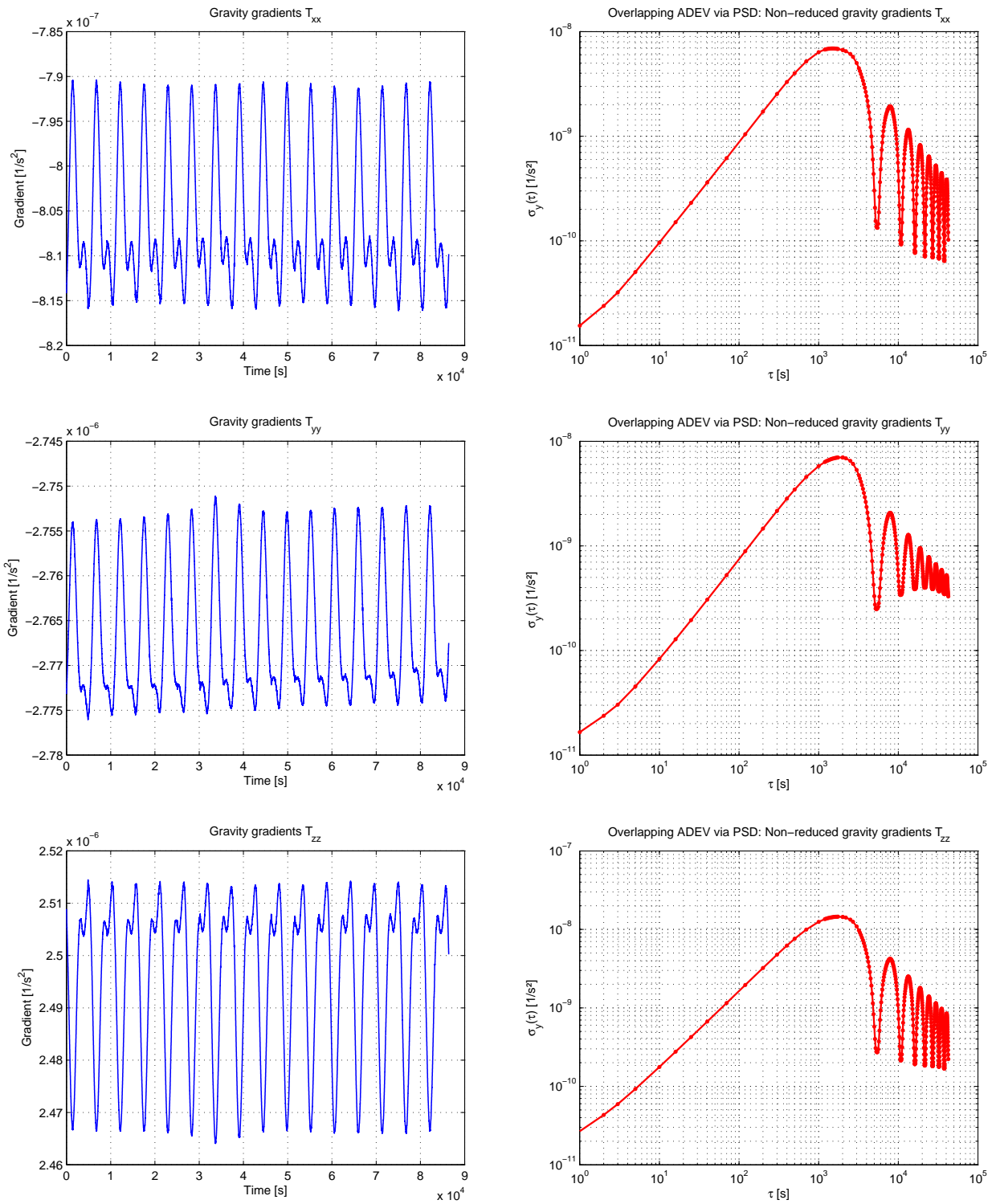


Figure 4.26: Original gravity gradients of the three main diagonal terms  $T_{xx}$ ,  $T_{yy}$ ,  $T_{zz}$  and their corresponding sigma-tau plots via PSD and transfer function

Figure 4.25 shows the result of the time-domain based ADEV calculation (right column) of the original gravity gradients (left column). The result of frequency-domain based ADEV calculation is shown by the red curves of figure 4.26. No pre-processing of data has been made, so that the obvious periodic contents are fully part of the ADEV calculation. All three  $\sigma - \tau$  plots have similar shape, which represents the so-called sinusoidal noise. But all of them include a frequency drift, too, represented by the rising straight line with slope +1, which ends at about the curve's maximum. Sinusoidal noise has the characteristics of dominating periodic interference. The curve's maximum, followed by further decreasing peaks, are the main characteristics. The amplitudes of the consecutive peaks usually fall off rapidly and can be approximated by an envelope with slope -1. Keeping all periodical content in the time series makes further noise identification difficult or even impossible, because of the large signal-to-noise ratio.

The above  $\sigma - \tau$  plots are governed by the orbit of GOCE. One orbit around the Earth takes about 5400 s. Adopting exactly this period for  $\tau$  — or a multiple of it — one obtains a minimum in the  $\sigma - \tau$  plot. Moreover, observation intervals  $\tau$  equal about the half of this period — or odd multiples of it — yield the maxima. Here, the differences of adjacent values in the ADEV computation algorithm become the biggest. More precisely, the absolute maximum is not located exactly at 2700 s, the half orbit period, but is a bit shifted to the left.

This behaviour is explained in detail in appendix B by means of a pure sinusoidal oscillation. In summary, filtering out the periodic content of the time series is helpful, if one is interested in extensive noise identification. But indeed, ADEV calculation and their graphic presentation proves to be also a possible tool for discovering trends and periodic interference. In above  $\sigma - \tau$  plots one even can easily read out the period of the time series by considering the minima and maxima.

Hence, the Allan deviation, especially if shown at all  $\tau$  values, can be considered as a form of spectral analysis. For this purpose one can consider the averaging interval  $\tau$  as the inverted frequency.

#### 4.5.2 GOCE gravity gradients $T_{xy}$

Finally, one off-diagonal term is analyzed as example. As before, reduced gravity gradients  $T_{xy}$  are created with the result that no trend or further periodic contents are observable.

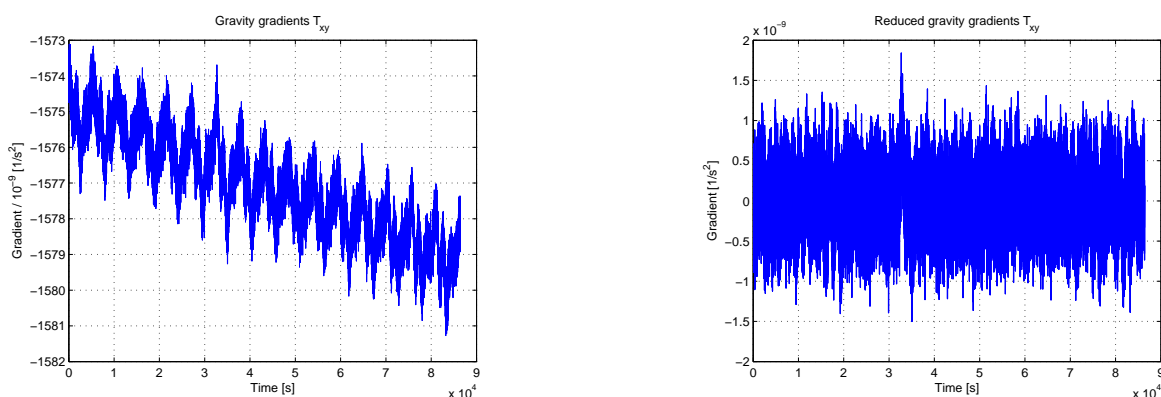


Figure 4.27: Original and reduced gravity gradients of the off-diagonal term  $T_{xy}$

The  $\sigma$ - $\tau$ -diagram depicts a downward curve with mostly negative slopes. The longer the observation interval  $\tau$  the more noise processes can be filtered out in regard to its stability. An absolute minimum cannot be detected because it just depends on the length of the time series. Hence the minimum will always be at the ending of the graph. The slope  $-\frac{3}{2}$  is predominantly and indicates White PM. In fact the data plot of the reduced gravity gradients resembles the simulated data plot for White PM bottommost in Figure 3.1.

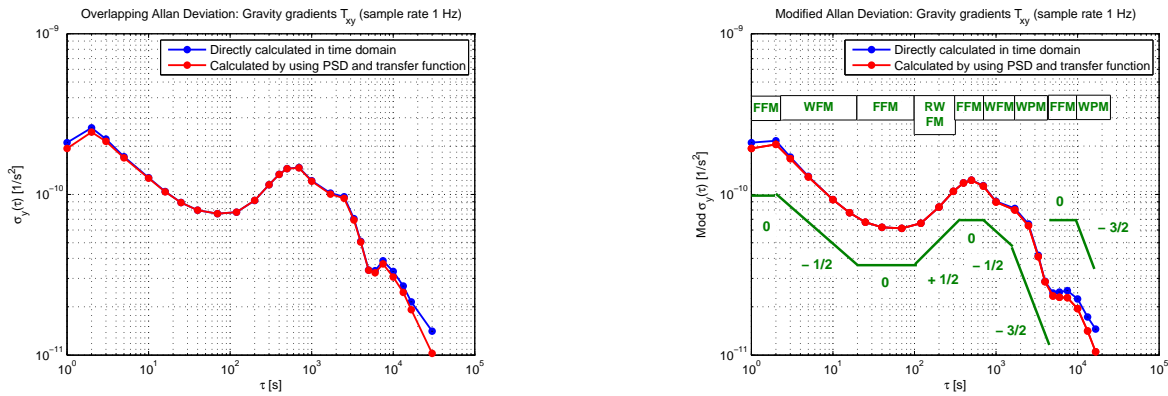


Figure 4.28:  $\sigma$ - $\tau$ -diagrams of the off-diagonal term  $T_{xy}$

At the very end, the original off-diagonal term without detrending or filtering out any periodic interference is analyzed. In comparison to the main diagonal terms, several noise types can be detected here, because periodic content is smaller (small signal-to-noise ratio) as in the main diagonal terms  $T_{xx}$ ,  $T_{yy}$  and  $T_{zz}$  and does not cover everything else.

White FM and Flicker FM are detected again. The sinusoidal noise becomes obvious in the small fluctuation between  $\tau = 1000$  s and  $\tau = 10000$  s. At about  $\tau = 5000$  s one attains to the minimum which originates from the orbital period of GOCE. The trend is clearly obvious at the end of the curve, that is in the rising straight line with slope  $+1$  (Figure 4.29), whereas the detrending causes the curve's final downgrade in the upper  $\sigma - \tau$  plot (Figure 4.28).

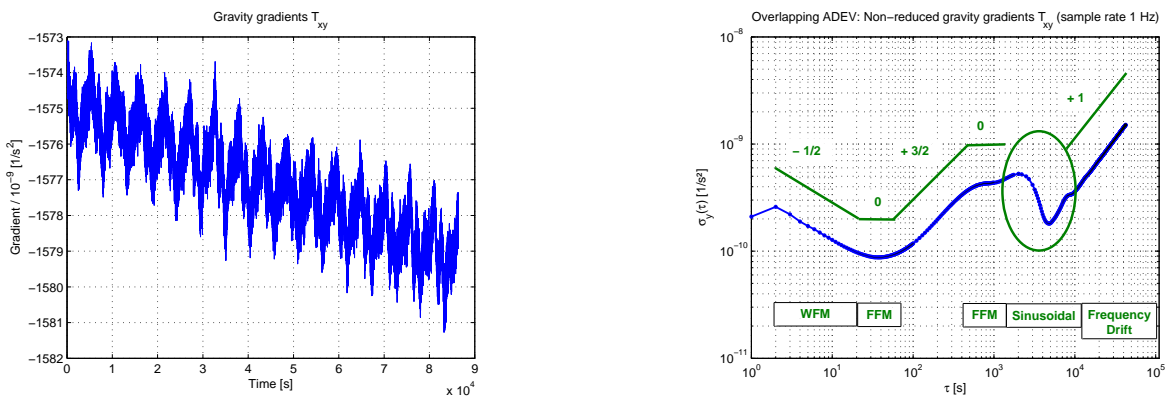


Figure 4.29:  $\sigma$ - $\tau$ -diagrams of the off-diagonal term  $T_{xy}$

## Chapter 5

### Discussion

The Allan variance is the most common time domain measure of frequency stability. In this student research project it is explained in detail how to compute the Allan variance. The difference between Allan variance and standard variance as well as further versions of the Allan variance are pointed out.

The methodology is quite simple and once programmed, it can be applied quickly to every type of time series. Contrary to the standard variance, the Allan variance is based on the summation over the squares of the distances of consecutive pairs of values. The aim of comprehensive Allan variance or Allan deviation calculation is not a single scalar, but an entire diagram because of the dependance on  $\tau$ . By means of this diagram, the most stable as well as the most instable points can be determined.

On the basis of the computed  $\sigma$ - $\tau$ -diagrams by own MATLAB files, different power law noise processes can be read out. Experience shows that in most cases, different noise terms appear in different regions of  $\tau$ . This allows identification of various random processes that exist in the data.

It is shown that it is possible to compute directly the Allan variance in the time domain as well as by the indirect way via power spectral density and a transfer function in the frequency domain.

Both methods operate well. The resulting  $\sigma$ - $\tau$ -diagrams always fit well together. It is observed that the diagrams computed by means of the power spectral density and the transfer function often takes a smoother course than its counterpart computed directly in time domain.

Conversion possibilities between the time domain and the frequency domain are demonstrated.

It is absolutely reasonable to apply the Allan variance to geodetic time series in order to analyze them. The Allan variance, or better the Allan deviation, especially if shown at all  $\tau$  values of interest, can be considered as a form of spectral analysis. Having said this, it is possible to consider the averaging interval  $\tau$  as the inverted frequency.

This circumstance become clear in case of time series with a large signal-to-noise ratio (here e.g. pole coordinates or the main diagonal terms of GOCE gravity gradients), where the ADEV will show minima and maxima. Minima occur at averaging times equal to integer multiples of the predominating period (vibration period).

Thus, the periodicity of a signal as well as a drift of a time series is reflected again in the corresponding  $\sigma$ - $\tau$ -diagram. One can recognize the behaviour and the course of a time series by considering the  $\sigma$ - $\tau$ -diagram.

If one is interested in noise type identification it is often necessary to reduce the signal-to-noise ratio by detrending or filtering out periodic or deterministic contents.

For instance, if one separates out computationally the known tide model of the gravimeter data, and only considers the remaining signal as gravimeter noise, one can analyze the gravimeter as a device and determine its stability and the existing noise processes.

For this purpose it is important to preprocess the data and to remove outliers, drifts or periodic contents. The idea is to make the signal as white as possible. This is necessary in order to ensure that preferably only noise processes are left over and to analyze just them. Otherwise one often obtains less suitable and strongly rising  $\sigma$ - $\tau$ -diagrams, which only indicate again, that a trend or periodic contents are present.

Finally, one arrives at the conclusion, that the Allan variance is a reasonable tool to analyze geodetic time series. The concept of the Allan variance fits well to the portfolio of a geodesist.

## Bibliography

- [1] David W. Allan. 'Statistics of Atomic Frequency Standards'. *Proceedings of the IEEE*, Vol. 54, No. 2, February 1966.
- [2] David W. Allan. David W. Allan's Time Interval Metrology Enterprise. Webpage, 2010. URL <http://www.allanstime.com>.
- [3] William J. Riley. Hamilton Technical Services. Webpage, 2010. URL <http://www.wriley.com>.
- [4] W. J. Riley. *Handbook of Frequency Stability Analysis*. National Institute of Standards and Technology (NIST), U.S. Department of Commerce, NIST Special Publication 1065, July 2008.
- [5] Timothy J.H. Craddock, Richard John Broderick, Colin P. Petersen, and Alex Hu. 'The GPS Toolkit: Open Source Clock Tools'. *40th Annual Precise Time and Time Interval (PTTI) Meeting*, 2008.
- [6] James A. Barnes et al. 'Characterization of Frequency Stability'. *IEEE Transactions on Instrumentation and Measurement*, Vol. IM-20, No. 2, May 1971.
- [7] P. Lesage and C. Audoin. 'Characterization and measurement of time and frequency stability'. *Reprinted in Radio Science*, Vol. 14, No. 4:521–539, 1979.
- [8] James A. Barnes and David W. Allan. 'Variances based on data with dead time between the measurements'. *NIST Technical Note 1318*, page 13, 1990.
- [9] Stefano Bregni. *Synchronization of Digital Telecommunications Networks*. John Wiley & Sons, Ltd, 2002.
- [10] David W. Allan, Neil Ashby, and Clifford C. Hodge. 'The Science of Timekeeping, Appendix A'. *Hewlett Packard Application Note 1289*, page 59, 1997.
- [11] David W. Allan. 'Time and Frequency (Time-Domain) Characterization, Estimation, and Prediction of Precision Clocks and Oscillators'. *IEEE Transactions on Ultrasonics, Ferroelectrics, and Frequency Control*, Vol. UFFC-34, No. 6, November 1987.
- [12] D.A. Howe, D.W. Allan, and J.A. Barnes. 'Properties of Signal Sources and Measurement Methods'. *Proceedings of the 35th Annual Symposium on Frequency Control*, 1981.
- [13] David W. Allan and James A. Barnes. 'A Modified "Allan Variance" with increased Oscillator Characterization Ability'. *Proceedings of the 35th Annual Frequency Control Symposium, USAERADCOM, Ft. Monmouth*, May 1981.
- [14] Paul Lesage and Théophane Ayi. 'Characterization of Frequency Stability: Analysis of the Modified Allan Variance and Properties of its Estimate'. *IEEE Transaction on Instrumentation and Measurement*, Vol. IM-33, No. 4:332–336, December 1984.

- 
- [15] Ulrich Bangert, DF6JB. 'Über die Stabilität von Oszillatoren und Frequenznormalen'. *AMSAT-Journal*. URL <http://ulrich-bangert.de/AMSAT-Journal.pdf>.
- [16] W.J. Riley and C.A. Greenhall. 'Power Law Noise Identification using the Lag 1 Auto-correlation'. *Preprint of paper to be presented at the 18th European Frequency and Time Forum, University of Surrey, Guildford, UK. 5 - 7 April 2004*.
- [17] Wilbur B. Davenport, Jr. and William L. Root. *An Introduction to the Theory of Random Signals and Noise*. Mc Graw-Hill Book Company, Inc., 1958.
- [18] E. Oran Brigham. *FFT - Schnelle Fourier-Transformation*. Oldenbourg, 6th edition, 1995.
- [19] 'IEEE Standard 647-1995: Format Guide and Test Procedure for Single-Axis Laser Gyros (Annex B and C)'. *IEEE Aerospace and Electronic Systems Society, USA, 1997*.
- [20] S.T. Dawkins, J.J. McFerran, and A.N. Luiten. 'Spectra and Variances (table)'. *IEEE Trans. UFFC 54(5)*, pages 918–925, May 2007.
- [21] Manfred Bauer. *Vermessung und Ortung mit Satelliten - GPS und andere satellitengestützte Navigationssysteme*. Herbert Wichmann Verlag, 5th edition, 2003.
- [22] Scintrex. *CG-5 Scintrex Autograv System - Operation Manual*, part no. 867700 revision 2 edition, 2007. Chapter 4.
- [23] Th. Gruber, R. Rummel, O. Abrikosov, and R. van Hees. *GOCE Level 2 Product Data Handbook*. The European GOCE Gravity Consortium (EGG-C), 2008.

## Appendix A

The two formulas (2.17) and (2.18) using frequency data  $\bar{y}$  and phase data  $x$  respectively are connected as follows. It starts with the basic formula for the first difference  $\bar{y}_i$  of a sequence of samples  $x_i$ :

$$\bar{y}_i = \frac{x_{i+1} - x_i}{\tau} \quad (2.7)$$

Assuming  $\tau$  equals the original sampling interval  $\tau_0$ , one obtains for the first differences  $\bar{y}_i, \bar{y}_{i+1}$  and  $\bar{y}_{i+2}$

$$\begin{aligned} \bar{y}_i &= \frac{1}{\tau_0} (x_{i+1} - x_i) && \iff && \frac{1}{\tau_0} x_{i+1} &= \bar{y}_i + \boxed{\frac{1}{\tau_0} x_i} \\ \bar{y}_{i+1} &= \frac{1}{\tau_0} (x_{i+2} - x_{i+1}) && \iff && \frac{1}{\tau_0} x_{i+2} &= \bar{y}_{i+1} + \frac{1}{\tau_0} x_{i+1} \\ &&& && &= \bar{y}_{i+1} + \bar{y}_i + \boxed{\frac{1}{\tau_0} x_i} \\ \bar{y}_{i+2} &= \frac{1}{\tau_0} (x_{i+3} - x_{i+2}) && \iff && \frac{1}{\tau_0} x_{i+3} &= \bar{y}_{i+2} + \frac{1}{\tau_0} x_{i+2} \\ &&& && &= \bar{y}_{i+2} + \bar{y}_{i+1} + \bar{y}_i + \boxed{\frac{1}{\tau_0} x_i} \\ &&& && \vdots & \vdots \\ &&& && \frac{1}{\tau_0} x_N &= \bar{y}_{N-1} + \bar{y}_{N-2} + \dots + \bar{y}_i + \boxed{\frac{1}{\tau_0} x_i} \end{aligned}$$

Note, that  $\boxed{\frac{1}{\tau_0} x_i}$  is a constant of integration.

Setting this constant of integration equal to zero in each case, yields:

$$\begin{aligned}
x_{i+1} &= \tau_0 \cdot \bar{y}_i \\
x_{i+2} &= \tau_0 \cdot (\bar{y}_i + \bar{y}_{i+1}) \\
x_{i+3} &= \tau_0 \cdot (\bar{y}_i + \bar{y}_{i+1} + \bar{y}_{i+2}) \\
x_N &= \tau_0 \cdot \sum_{i=1}^{N-1} \bar{y}_i \\
x_{i+m} &= \tau_0 \cdot \left[ \sum_{j=1}^i \bar{y}_j + \sum_{j=i+1}^{i+m-1} \bar{y}_j \right] \\
x_{i+2m} &= \tau_0 \cdot \left[ \sum_{j=1}^i \bar{y}_j + \sum_{j=i+1}^{i+2m-1} \bar{y}_j \right]
\end{aligned}$$

Now, one inserts the necessary terms into equation (2.18):

$$\begin{aligned}
& \frac{1}{2(N-2m)\tau^2} \sum_{i=1}^{N-2m} [x_{i+2m} - 2x_{i+m} + x_i]^2 \tag{2.18} \\
&= \frac{\tau_0^2}{2(N-2m)\tau^2} \sum_{i=1}^{N-2m} \left[ \sum_{j=1}^i \bar{y}_j + \sum_{j=i+1}^{i+2m-1} \bar{y}_j - 2 \sum_{j=1}^i \bar{y}_j - 2 \sum_{j=i+1}^{i+m-1} \bar{y}_j + \sum_{j=1}^{i-1} \bar{y}_j \right]^2 \\
&= \frac{\tau_0^2}{2(N-2m)\tau^2} \sum_{i=1}^{N-2m} \left[ \sum_{j=1}^{i-1} \bar{y}_j + \sum_{j=i}^{i+2m-1} \bar{y}_j - 2 \sum_{j=1}^{i-1} \bar{y}_j - 2 \sum_{j=i}^{i+m-1} \bar{y}_j + \sum_{j=1}^{i-1} \bar{y}_j \right]^2 \\
&= \frac{\tau_0^2}{2(N-2m)\tau^2} \sum_{i=1}^{N-2m} \left[ -2 \sum_{j=i}^{i+m-1} \bar{y}_j + \sum_{j=i}^{i+m-1} \bar{y}_j + \sum_{j=i+m}^{i+2m-1} \bar{y}_j \right]^2 \\
&= \frac{\tau_0^2}{2(N-2m)\tau^2} \sum_{i=1}^{N-2m} \left[ - \sum_{j=i}^{i+m-1} \bar{y}_j + \sum_{j=i+m}^{i+2m-1} \bar{y}_j \right]^2 \\
&= \frac{\tau_0^2}{2(N-2m)\tau^2} \sum_{i=1}^{N-2m} \left[ - [\bar{y}_i + \bar{y}_{i+1} + \dots + \bar{y}_{i+m-1}] + \bar{y}_{i+m} + \bar{y}_{i+m+1} + \dots + \bar{y}_{i+2m-1} \right]^2 \\
&= \frac{\tau_0^2}{2(N-2m)\tau^2} \sum_{i=1}^{N-2m} \left[ \bar{y}_{i+m} + \bar{y}_{i+m+1} + \dots + \bar{y}_{i+2m-1} \right. \\
&\quad \left. - \bar{y}_i - \bar{y}_{i+1} - \dots - \bar{y}_{i+m-1} \right]^2
\end{aligned}$$

Interchanging the indices yields

$$= \frac{\tau_0^2}{2(N-2m)\tau^2} \sum_{j=1}^{N-2m} \left\{ \sum_{i=j}^{j+m-1} (\bar{y}_{i+m} - \bar{y}_i) \right\}^2$$

with  $\tau = m \cdot \tau_0$  and  $N = M + 1$ :

$$= \frac{1}{2m^2(M-2m+1)} \sum_{j=1}^{M-2m+1} \left\{ \sum_{i=j}^{j+m-1} (\bar{y}_{i+m} - \bar{y}_i) \right\}^2 \tag{2.17}$$

## Appendix B

This appendix contains explanations about the sinusoidal noise. A pure sinus signal  $y = \sin\left(\frac{2\pi t}{T}\right)$  is assumed as time series with period  $T$  and normalized amplitude 1, as plotted in figure B.1:

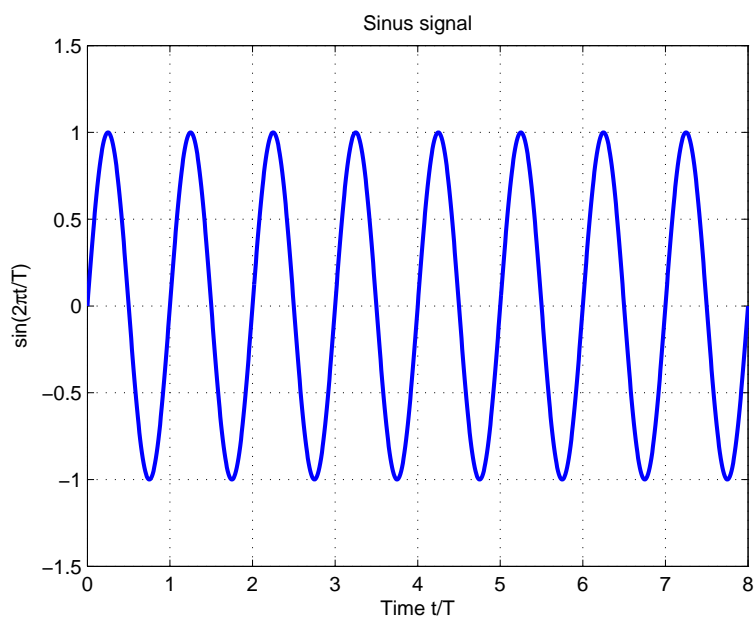


*Figure B.1: Sinus signal*

Using the ADEV algorithm yields the sigma-tau plot depicted in figure B.2. The maximum lies at  $\tau/T \approx 0.371$ . This matter of fact shall be explained in this appendix.

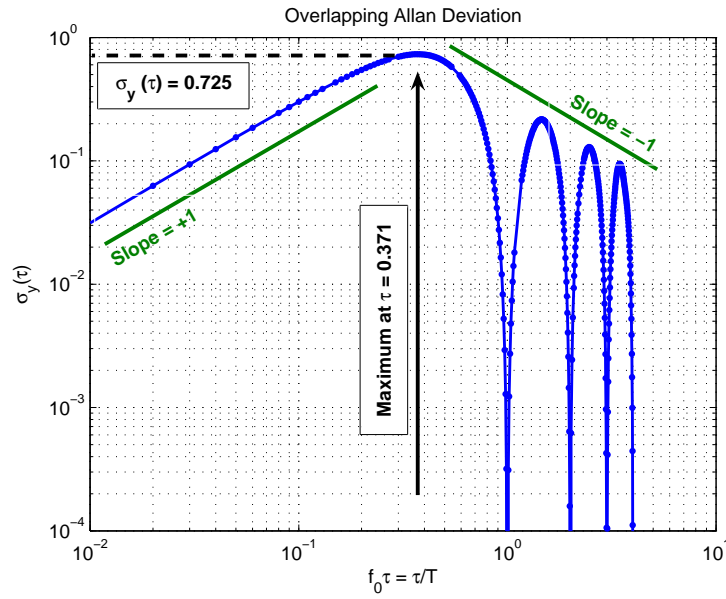


Figure B.2: sigma-tau plot for the sinus signal

The ADEV is computed via power spectral density (PSD) and the given transfer function. A representation of the PSD of the above sinus signal containing a single frequency is given as:

$$S_{\Omega}(f) = \frac{1}{2} \Omega_0^2 [\delta(f - f_0) + \delta(f + f_0)]$$

where  $\Omega_0$  is the amplitude  
 $f_0$  is the frequency  
 $\delta(x)$  is the Dirac delta function.

The adequate formula for ADEV computation is

$$\sigma^2(\tau) = 2 \int_0^{f_h} S_{\Omega}(f) \cdot \frac{\sin^4(\pi\tau f)}{(\pi\tau f)^2} df.$$

Inserting the PSD of the sinus signal yields

$$\begin{aligned} \sigma^2(\tau) &= \Omega_0^2 \int_0^{f_h} [\delta(f - f_0) + \delta(f + f_0)] \cdot \frac{\sin^4(\pi\tau f)}{(\pi\tau f)^2} df \\ &= \Omega_0^2 \int_0^{f_h} \delta(f - f_0) \cdot \frac{\sin^4(\pi\tau f)}{(\pi\tau f)^2} df + \Omega_0^2 \int_0^{f_h} \delta(f + f_0) \cdot \frac{\sin^4(\pi\tau f)}{(\pi\tau f)^2} df \\ &= \Omega_0^2 \int_0^{f_h} \delta(f - f_0) \cdot \frac{\sin^4(\pi\tau f)}{(\pi\tau f)^2} df \\ &= \Omega_0^2 \frac{\sin^4(\pi\tau f_0)}{(\pi\tau f_0)^2} \end{aligned}$$

according to the sifting integral

$$I = \int_{-\infty}^{+\infty} f(x_0) \delta(x - x_0) dx$$

where  $f(x)$  is continuous at  $x_0$ . From the properties of the unit impulse function, the integrand of  $I$  is nonzero only at the point  $x = x_0$ . The only contribution of  $f(x)$  to the integral is thus at the point  $x = x_0$ , and one can write

$$I = f(x_0) \int_{-\infty}^{+\infty} \delta(x - x_0) dx = f(x_0).$$

Hence, the ADEV of the sinus signal is

$$\sigma(\tau) = \Omega_0 \frac{\sin^2(\pi\tau f_0)}{\pi\tau f_0}.$$

Looking for the maximum of this function, demands the derivative with respect to  $\tau$

$$\frac{d\sigma}{d\tau} = \frac{\pi f_0 \cdot \sin(\pi f_0 \tau)}{(\pi f_0 \tau)^2} \left[ 2\pi f_0 \tau \cos(\pi f_0 \tau) - \sin(\pi f_0 \tau) \right]$$

1st solution:  $\sin(\pi f_0 \tau) = 0 \Rightarrow f_0 \tau = k$  with  $k = 0, 1, 2, \dots, N$ .

2nd solution:

$$\begin{aligned} \sin(\pi f_0 \tau) &= 2\pi f_0 \tau \cos(\pi f_0 \tau) \\ 2\pi f_0 \tau &= \tan(\pi f_0 \tau) \end{aligned}$$

This equation is solved graphically in figure B.3. The solutions are depicted as black circles.

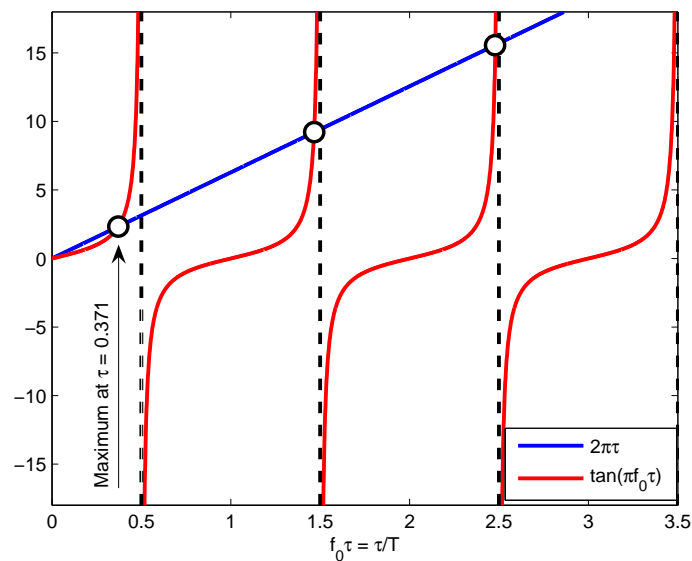


*Figure B.3: Graphical solution of the determination of the maximum*

The first point of intersection is located at  $f_0\tau \approx 0.371$  and is responsible for the absolute maximum in the sigma-tau plot of the sinus signal. The points of intersection number two and three are depicted by circles, too. These intersections are both closer to the vertical asymptote as the first circle. All further intersections are located closer and closer to the corresponding asymptotes because of the arising straight line (blue). They determine the sub-maxima in figure B.2.



# Appendix C

In this appendix the MATLAB source code filenames will be listed with a short explanation what each file does.

All the MATLAB source codes as well as the data of the analyzed time series have the directory `matlab` as root directory.

## C.1 Calculation of the sigma-tau diagrams for non-overlapping, overlapping and modified Allan deviation (Time-Domain-Based)

- `allan20.m` – computes the non-overlapping Allan deviation
- `allan_overlap20.m` – computes the overlapping Allan deviation
- `allan_modified10.m` – computes the modified Allan deviation

## C.2 Calculation of the sigma-tau diagrams for overlapping and modified Allan deviation (Frequency-Domain-Based)

- `spectrum.m` – computes the one-sided psd with full power of a time series via FFT
- `psd2ADEV.m` – computes the overlapping Allan deviation using the one-sided psd and a transfer function
- `psd2modADEV.m` – computes the modified Allan deviation using the one-sided psd and a transfer function

## C.3 Main programs for the analysis of geodetic time series

- `main_oscillator.m` – Analysis of oscillator frequencies
- `main_EOP_pole_x.m` – Analysis of the  $x$ -component of the pole
- `main_EOP_pole_y.m` – Analysis of the  $y$ -component of the pole
- `main_GPS_absolutevalues.m` – Analysis of absolute values of complex GPS position data

- `main_GPS_arguments.m` – Analysis of arguments of complex GPS position data
- `main_gravimeter.m` – Analysis of Scintrex CG-5 Gravimeter data
- `main_gravimeter_detrended.m` – Analysis of detrended Scintrex CG-5 Gravimeter data
- `main_GOCE_Txx_filtered.m` – Analysis of filtered GOCE gravity gradients  $T_{xx}$
- `main_GOCE_Tyy_filtered.m` – Analysis of filtered GOCE gravity gradients  $T_{yy}$
- `main_GOCE_Tzz_filtered.m` – Analysis of filtered GOCE gravity gradients  $T_{zz}$
- `main_GOCE_Txy_filtered.m` – Analysis of filtered GOCE gravity gradients  $T_{xy}$
- `main_GOCE_Txx.m` – Analysis of GOCE gravity gradients  $T_{xx}$
- `main_GOCE_Tyy.m` – Analysis of GOCE gravity gradients  $T_{yy}$
- `main_GOCE_Tzz.m` – Analysis of GOCE gravity gradients  $T_{zz}$
- `main_GOCE_Txy.m` – Analysis of GOCE gravity gradients  $T_{xy}$

#### C.4 Additional helper functions

- `nmealineread.m` – reads an NMEA sentence into a MATLAB structure array
- `fourier_coefficients.m` – determines the coefficients of a Fourier series for the GOCE main diagonal terms
- `fourier_coefficients_XY.m` – determines the coefficients of a Fourier series for the GOCE off-diagonal term